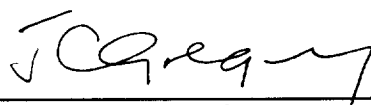/N · 93-~R

Final Report

on NASA Grant NAGW-2023

A Measurement of the Energy Spectra of Cosmic Rays from 20 to 1000 GeV Per Amu

J. C. Gregory, C. Thoburn, A. E. Smith, and J. J. Petruzzo III, University of Alabama at Huntsville, Huntsville, AL, 35899, USA
R. W. Austin and J. H. Derrickson and T. A. Parnell, George C. Marshall Space Flight Center, AL 35812, USA
M. R. W. Masheder and P. H. Fowler, H.H. Wills Physics Laboratory, University of Bristol, BS8 1TL, United Kingdom

J.C. Gregory
Chemistry Department
The University of Alabama in Huntsville
Huntsville, AL   35899

November 1997

Table of Contents

A Measurement of the Energy Spectra of Cosmic Rays
from 20 to 1000 GeV Per Amu

Summary of Program

The original BUGS4 instrument was designed and partly built in Bristol (United Kingdom) in the 1980's. In 1990 it was shipped to the University of Alabama in Huntsville, Alabama, where it was completely refurbished, calibrated and prepared for flight. A new electronics system (which was designed and built at NASA Marshall Space Flight Center) was installed. This project was funded in the U.S. by the Office of Space Science, NASA. Collaborators on the project were UAH, NASA Marshall Space Flight Center and the University of Bristol. A round-the-world flight of the detector was planned in order to collect the cosmic ray statistics required for our astrophysical purpose, but prior to this an engineering flight was scheduled and performed from Ft. Sumner, New Mexico in September 1993. This flight was successful in demonstrating the proof-of-principle of several novel detector techniques. However, the instrument was completely destroyed during landing and resources for rebuilding were not available.

Several publications were written describing the results and a Ph.D. degree in physics was awarded based on the research.

Results from the Project

a)   **Scientific and Technical.** Project achievements have been reported in both refereed and archival conference proceedings, as follows:

Design and Flight Performance of the Cosmic Ray Detector BUGS-4, A.E. Smith, J.J. Petruzzo III, J.C. Gregory, C. Thoburn, R.W. Austin, J.H. Derrickson, T.A. Parnell, M.R.W. Masheder, P.H. Fowler, **Nucl. Instrum. Meth. Phys. Res.** 402 (1) (1998) 104-122.

A One-Meter Radius Spherical Drift Chamber for the Measurement of Relativistic Heavy Nuclei, J.J. Petruzzo III, A.E. Smith, J.C. Gregory, C. Thoburn, R.W. Austin, T.A. Parnell, J.H. Derrickson, M.R.W. Masheder, P.H. Fowler, **Nucl. Instrum. Meth. Phys. Res.** 402 (1) (1998) 123-138.

Results from the Flight of BUGS IV, A.E. Smith, J.J. Petruzzo III, J.C. Gregory , J.H. Derrickson, T.A. Parnell, M.R.Wm. Masheder, P.H. Fowler , **24th International Cosmic Ray Conference**, Rome, Italy, August 28-September 8, 1995, Vol. 3, OG10.3.6, p. 587.

Performance of Bugs IV Spherical Drift Chamber, J.J. Petruzzo III, A.E. Smith, J.C. Gregory , J.H. Derrickson, T.A. Parnell , M.R.Wm. Masheder,

P.H. Fowler , **24th International Cosmic Ray Conference**, Rome, Italy, August 28-September 8, 1995, Vol. 3, OG10.3.6, p. 637.

An Instrument to Measure the Energy Spectra of Cosmic Rays from 20 to 1000 GeV per amu, P.H. Fowler, J.C. Gregory, C. Thoburn, T.A. Parnell, R.W. Austin,J.H. Derrickson, M.R.W. Masheder and J.W. Watts. **Papers of the 22nd International Cosmic Ray Conference**, Dublin, eds. The Dublin Institute for Advanced Studies, Volume 2, Pages 587-590, 11-23 August 1991.

Measurement of the Primary Cosmic Ray Spectra, J. Petruzzo, Dissertation for Ph.D. in Physics, University of Alabama in Huntsville, Spring 1996.

b)   Education and Training

1.   Dr. Joseph J. Petruzzo III received his Ph.D. in Physics (1996) from UAH based on this work (see references in (a) above).

2.   Val Byler worked as an undergraduate assistant on the project for three years. He received his B.S. in Physics in 1995, and partly based on his extensive practical experience with our group, he was immediately employed by a local high-tech company.

A Measurement of the Energy Spectra of Cosmic Rays
from 20 to 1000 GeV Per Amu

NAGW-2023

SUMMARY

The design features and operational performance from the test flight of the fourth generation of spherical geometry cosmic ray detectors developed at Bristol University (Bristol University Gas Scintillator 4 -- BUGS-4) are presented. The flight from Ft. Sumner (NM) in Sept. 1993 was the premier flight of a large (1m radius) spherical drift chamber which also gave gas scintillation and Cerenkov signals. The combinations of this chamber with one gas and two solid Cerenkov radiators lead to a large aperture factor (4.5 m2sr), but low (~3.5 g/cm2) instrument mass over the energy sensitive range 1 to several hundred GeV/a. Moreover, one simple timing measurement determined the impact parameter which provided a trajectory (path length) correction for all detector elements. This innovative and efficient design will be of interest to experimental groups engaged in studies of energetic charged particles. Although there were technical problems on the flight, which were compounded by the total destruction of BUGS-4 by fire while landing in Oklahoma, there was a period of stable operation during which the instrument was exposed at float altitude (~ 125,000 ft.) to high energy cosmic rays. We present the performance of the instrument as determined from the analysis of these data and an appraisal of its novel design features. Suggestions for design improvements in a future instrument are made.

1. Introduction

We describe the BUGS-4 (Bristol University Gas Scintillator mark-IV) instrument (section 3) and present the flight performance. Some performance features are well below the design expectations due to several technical problems including interference from ballast commands that arbitrarily changed the remote commandable photo-multiplier voltages. Due to these problems we have limited analysis to a small subset of good data (30,000 events -- the first ~ 90 minutes) when no commands were sent. We show from these data that the design concept worked well and note features compromised by the technical difficulties and others that can be improved. In this paper we concentrate on the overall performance. Since a detailed discussion of the central drift chamber does not easily fit into this paper it is presented in a separate paper (Petruzzo et al.)[1]. We discuss specific analysis techniques that may have general application for similar devices in section 4 and present the results of this detailed analysis in section 5 before concluding in section 6.

To provide a context for the instrument performance discussion in section 2.1 we briefly review the intended scientific objectives of BUGS-4. In section 2.2 we demonstrate the merits of BUGS-4 by making comparisons with contemporary instruments and show how well suited the design concept was to an area of high scientific interest.

4

2. Cosmic rays and contemporary detectors

2.1 Current topics of interests in the study of galactic cosmic rays

The measured flux of galactic cosmic rays contains the nuclei of all the chemical elements along with small amounts of e- (~1%) and e+ (~0.1%). The energy range extends from hundreds of MeV to > 10^{20} eV. Contemporary experimental study of galactic cosmic rays (below ~10^{15} eV) addresses three main questions: In what source(s) are cosmic rays produced? What is (are) the mechanism(s) operating in the accelerator(s)? What governs the propagation of cosmic rays through the galactic inter-stellar medium (ISM) and leakage from the galaxy? Each of these questions divides into a variety of inter-linked topics that illuminate many areas of contemporary astronomy in ways that are not otherwise accessible.

Due to the enormous range in energy and species the instruments required to address specific topics differ. In the energy regime up to ~1000 GeV/a there are several interesting issues. The ratio of the primary to secondary (produced by hadronic interactions between primary cosmic rays and the galactic ISM) decreases with energy due to two competing processes. The higher energy cosmic rays are less scattered by the galactic magnetic fields and arrive more quickly having transversed less of the galactic ISM. However, such cosmic rays are also more likely to leak from the galaxy.

It is only from direct measurement that various theoretical models, incorporating these features, can be refined and constraints on the source established. At lower energies the primary to secondary ratios have been used to refine propagation models[2]. However, low energy data are compromised by solar modulation and by the energy dependence of the interaction cross-sections. The experimental work at higher energies (>50 GeV/a) [3,4,5] has been limited both by statistics and by concerns over detector calibration. However, these data indicate an enrichment of iron and extrapolation[5] to the all particle spectrum measured in the range 10^{13}-10^{14} eV indicates about 25% (by number) of the cosmic-rays have $Z \geq 6$. This may reflect that the large abundance of protons and helium at lower energies comes from a different source. Equally suggestive of multiple sources is the observation in two independent experiments[2,3] that silicon falls off more rapidly than other species, although this may still be a three standard deviations effect. To progress further data of good statistical quality with good element and energy resolution is needed.

2.2 Contemporary Instruments

The design of cosmic ray detectors is driven by three often conflicting requirements: large aperture, since exposure times are limited and the flux of cosmic rays is small; low mass, so that energy degradation and the background from nuclear interactions are minimized; and trajectory determination to correct the detector response for the random flux orientation. The instruments must also resolve element species (and for some experiments isotopes) and have good energy resolution. The instrument must be light enough to be lifted either into orbit by rocket or sub-orbit beneath a stratospheric balloon, rugged enough to tolerate the operating environment and be commandable remotely.

BUGS-4 was designed to measure the charge (oxygen to iron) and energy spectrum from one to several hundred GeV/a of the primary galactic cosmic rays. A unique innovation was a large (1m radius) spherical drift chamber. This new technique, coupled with refinements from three previous instruments, lead to a device both of exceptionally large aperture (4.5 m2sr) and low mass (~ 3.5 g/cm2).

To put these numbers into context we show the parameters (Table 1) of BUGS-4 and the three most cited contemporary active instruments. (HEAO-3-C2[6], HEAO-3-HNE[7] and CRN[3,8].

From Table 1 it is evident that the BUGS-4 aperture and mass thickness compares favorably with these instruments. Only CRN offered a similar charge and energy range to BUGS-4. Unfortunately a re-flight of CRN to improve the statistics is still in the future. The primary disadvantage of BUGS-4 is the residual atmosphere above the instrument that is inherent to balloon exposures. However the unique design so minimizes instrument structure that the effective mass (instrument and atmosphere) and consequent cosmic ray slowing and nuclear fragmentation are not prohibitive. An eight day exposure of BUGS-4, commonly achieved in long duration ballooning, would give a 8¥(4.5/1.93) ~ 19 fold increase over the iron data set from the CRN experiment. Moreover, the energy sensitivity in BUGS-4 came from detectors with overlapping energy response (see section 3.1) thereby reducing normalization uncertainties.

3.   The BUGS-4 Detector

BUGS-4 is shown schematically in Figure 1. To provide a framework for the detailed discussions of each region we first overview the modus operandi. Each distinct region: A, B and C are then described in detail. The mechanical assembly and material dimensions are given in appendix A; the electronics in appendix B. Finally to provide a context for discussing the flight performance, which due to operational problems was worse than expected, the design performance is presented.

3.1   Modus Operandi of BUGS-4

All signals in BUGS-4 were optical: Cerenkov and gas scintillation; no electrical current measurements were made. A schematic diagram of the signals in each region of Bugs-4 is shown in Figure 2. A cosmic ray, transversing the Pilot 425 Cerenkov radiators in regions A and C (The trigger was a coincidence between A and C, -- see appendix B), also generates a prompt primary optical scintillation signal (l~350 nm) from an excited argon atom and nitrogen molecule interaction in the drift chamber (region B). Electrons liberated along the primary track drift to the central electrode (held at 3 kV) where they gain sufficient energy from the field to produce further optical emission through the mechanism of gas proportional scintillation. The drift time is approximately proportional to the square of the impact parameter (see section 3.3) and can be determined to ~ 3mm by timing the arrival of the electrons relative to the prompt primary scintillation. This single measurement provides a trajectory correction for all detector elements -- see section 5.1. Energy sensitivity came from solid Pilot-425 Cerenkov radiators (threshold ~ 0.4 GeV/a), a Freon gas (Freon 12 -- CF_2Cl_2) Cerenkov radiator in region C (threshold ~ 20 GeV/a), and argon in B (threshold ~ 70 GeV/a). These overlapped the rise in specific energy loss in region B thus providing internal cross calibration. The relativistic rise in the prompt scintillation signal extends the energy resolution to several hundred GeV/a.

3.2   Region A

This region provided the primary charge determining element from the Cerenkov light liberated by cosmic rays transversing a 6 mm layer of Pilot 425 (refractive index (n) of 1.518 ±0.005[9] which was arranged in 43 tessellations and mounted on the outer upper surface of region B to create a dome like structure. A hole was left at the pole to accommodate the central drift electrode in region B -- see section 3.3. The cavity, which was coated with $BaSO_4$, was viewed by sixteen photo-multipliers, grouped in pairs; each

with a fish eye lens. This arrangement gave a measured detection efficiency for light from a green LED placed near the pole of ~7.25 photo-electrons per 100 photons. The detection efficiency has a position dependence that is discussed in section 4.1.

Region A was designed to produce a signal that was practically all Cerenkov for the smallest path lengths. Potential background light was produced from parasitic scintillation in the Pilot or from the ~40 cm of air above the Pilot. The expected background has previously been established experimentally by Tarle *et al.*[10]. This was for a different experiment but the results are useful here. Tarle et al.[10] estimate that for relativistic (b=1) particles the scintillation components of 1.27 cm of Pilot (twice the thickness of Region A) and the 38 cm of air is only ~ 2 % and ~ 1% respectively. Although the scintillation components for near Cerenkov threshold events is a large fraction of the Cerenkov signal, events of such low energy could not reach the instrument. The geomagnetic cut-off at the launch site (Fort Sumner, New Mexico) was 4.10 GV, corresponding to a vertical cut-off kinetic energy for iron-56 of 1.19 GeV/a. Hence the signals measured in region A were, to an excellent approximation, purely Cerenkov and proportional to $Z_2¥(1- b_{-2} n_{-2})$; Z is the species charge.

3.3   Region B

Region B had three functions: a gas scintillation chamber, a drift chamber and a gas Cerenkov detector. These signals occur in different time regimes: The Cerenkov signal peaks (10 to 90%) in ~ 5ns, the gas scintillation in 50 ns and the drift times extend from a few to ~ 700 m-seconds. An innovative FET photo-multiplier base that extracted all these signals from each photo-multiplier was developed[13].

A cosmic ray transversing region B leaves a trail of ionized and excited atoms. Due to composition of the gas (200 torr argon, 50 torr helium, and 1.5 torr of nitrogen) and the cross-sections for interactions with the cosmic rays, an ensemble of predominantly argon ions, excited argon atoms and electrons is produced along the track of each cosmic ray. An interaction between the excited argon atoms (not argon ions) and nitrogen molecules results in the excitation of the nitrogen molecules which after ~ 38 ns emits a broad spectrum in the range 337 - 520 nm; see Petruzzo *et al.* [1].

In previous BUGS instruments corrections for the signal path length dependence have utilized phenomenological techniques: for example using the biggest/mean[17] signals to estimate the trajectory or by geometric techniques[11] to minimize it. To progress further with larger aperture instruments, that are required to study the weaker fluxes at higher energies, a direct measurement of the path length was needed. BUGS-4 was the first BUGS instrument with a spherical drift chamber[12] that enabled the path length to be measured. A one meter long ceramic probe[13] was constructed such that the electrical field gradient matched the r_{-2} field for a point charge. A 5.08 cm diameter rhodium plated hollow sphere was attached to the end of the probe which was suspended from the pole of region B such that the two-inch sphere was at the center of this region.

Electrons liberated along the track of a cosmic ray drift to the central electrode which was held at 3 kV. This voltage is too low for charge multiplication. The electron drift time is a function of the voltage on the central electrode, the impact parameter and the gas composition. A full description including the effects of diffusion and inelastic excitation, and how these properties affect the drift time, and the wave-form shape is provided by Petruzzo *et al* [1]. Here we summarize the salient points. For a given electrode voltage and impact parameter, the drift is dominated by the electron-gas momentum cross-sections. Argon has a characteristic Ramsauer effect and is practically transparent to electrons at ~ 0.3 eV. Helium, which has an electron collision cross-section that is essentially energy

independent was added to the gas mixture so that the drift times do not have a strong energy dependence. For large impact parameters (p) the drift time increases from the p_2 dependence found at small p; this has been modeled[1]. The relation of p to the path lengths through the detector elements in regions A (C, not displayed, is similar to A) and B is shown in Figure 3.

The atomic processes involved in the GPS process are somewhat different from those producing the primary scintillation. The drifting electrons have a low energy until they reach the vicinity of the central electrode where the electric field is high; only then will their kinetic energy, even in the high velocity tail, approach the ~11 eV for the appropriate excitations to occur. In the scintillating gas mixture it is the nitrogen that dominates the GPS as it has the lowest energy threshold. The magnitude of the emission is optimized by altering the drift voltage (V); empirically it is found that the yield varies as V_3 over a considerable range from just above threshold. The amount of nitrogen is chosen to optimize the primary scintillation yield, its time structure and the total drift time which decreases steadily with increasing nitrogen. With the chosen mixture and 3 kV applied to the central electrode the GPS was ~ 30 times the primary scintillation; more details are presented by Petruzzo et al [1].

The surface treatment applied in region B to optimize its optical properties were different to those used in regions A and C. $BaSO_4$ could not be applied to the inner surfaces of region B since the parasitic scintillation would swamp the gas Cerenkov signal. $BaSO_4$ was applied around the inner belly band since coincident cosmic rays could not strike this surface. The upper and lower inner dome surfaces were bead-blasted to create a diffuse reflector and chemically brightened (see appendix A).

The optical signals in region B were detected by eight five-inch diameter Hamamatsu RA-1250 photo tubes. These tubes were used since they have fast rise times (~2 ns), a uniform position response across the photo-cathode and small transit time jitter. The voltages for the photo-tubes were provided via active FET base circuits that enabled both the fast and slow signals to be measured -- see Appendix B. To minimize disturbances to the drift field each tube was placed behind a fine wire grid that was grounded to the central chamber to screen the drift field from the photo-tube high-voltages. To improve the light collection each tube was equipped with a 12-inch diameter Pilot 425 aerial – see Figure 4. Each aerial was coated with a compound containing p-Terphenyl-BIS-MSB to enhance the wavelength conversion (UV to blue) efficiency. The detection efficiency was measured by directing a weak UV laser pulse directly into a photo-tube equipped with an aerial and then shining the same laser directly on to the floor of region B. The ratio of these signals gave an efficiency of ~ 4 p.e. for every 100 UV photons.

Although the good data contained too few gas Cerenkov events to analyze we briefly discuss the technique employed to measure the gas Cerenkov signal. Due to the characteristic light collection time in region B (~ 18 ns) the gas Cerenkov signal overlaps the leading edge of the prompt gas scintillation signal -- see Figure 5. To separate them a ladder filter was used with a fast Le-Croy ADC to take 12 equally spaced (10ns) samples of the leading edge. Simulations that were refined using the measured response of the photo-tubes to a fast UV laser indicate that the Cerenkov component can be recovered by using a weighted sum of the wave-form samples. A similar technique was used to analyze data from the Bristol experiment aboard the Ariel 6 satellite[9].

Before flight region B was evacuated to ~ 10 milli-torr then back filled with the flight gases. Due to the huge volume (4.6 m3) of region B a miniature version of the chamber (mini-BUGS) was used for testing and optimizing gas mixtures. Since the mixture was sensitive to nitrogen this was introduced first and its pressure measured with a

gauge specifically calibrated for nitrogen. The energy dependence of the optical scintillation emission of the flight gas was calibrated with a spectral 252Cf source; details are presented by Petruzzo *et al* [1] (next paper in this journal).

3.4 Region C

This cavity is similar to region A, but it also contained a Freon Cerenkov radiator with a threshold of ~ 20 GeV/a. The Pilot Cerenkov radiator was 1.5 mm thick (25% of that in region A) so that the Pilot and Freon gas Cerenkov signals were of similar amplitude. As there was no probe mount all the upper surface of region C (outer bottom of region B) was clad. Each tessellation was larger: 16, as against 43 in A, were used to create a similar area to region A. The stable data contains few Freon Cerenkov events; they are not discussed.

3.5 The design performance

Due to the ballast command interference, that lead to a loss of the photo-tube balance and serious systematic errors, the measured element and energy resolution were well below the design expectations. From the results of the analysis it is also suspected that the tessellation frosting was not optimized. Here we discuss the expected performance to provide a context for the flight performance and to enable an evaluation the design.

The energy and charge resolution both depend on the energy of the cosmic rays. First we consider the region between the Cerenkov threshold of ~ 0.4 GeV/a to minimum ionizing particles at ~ 2 GeV/a (note that in the data presented here the geomagnetic cut-off limits the minimum detectable cosmic rays to ~ 1.1 GeV/a). The Pilot Cerenkov signal in region A increases while the gas scintillation signal in region B decreases. The cosmic-ray charge can be determined from the analytical expressions for these two signals by eliminating the velocity dependence. A similar technique was employed to analyze data from the Bristol cosmic ray detector on the Ariel 6 satellite[9]. BUGS-4 had the advantage that the impact parameter was directly measured. Simulations suggest a charge resolution of ~ 0.2 units (one sigma) can be achieved[10]. Similar charge resolution can also be achieved for cosmic rays that exceeded the Freon gas Cerenkov threshold (~ 20 GeV/a).

The worst charge resolution is between minimum ionization (~ 2 GeV/a) and the Freon Cerenkov threshold (~ 20 GeV/a). In this regime the experiment is relatively insensitive to energy. Although beyond ~ 4.5 GeV/a the Cerenkov signal in region A has saturated, the energy determined from the scintillation signal in region B is ambiguous and it is not possible, for example, to differentiate between a iron cosmic ray (Z=26) of energy g=2 and a manganese (Z=25) cosmic ray of energy g=17. It is best to assume that each primary has an effective g equal to the median of the group ~ 7. The maximum error in the charge resolution can be obtained by substituting the two extreme energy values of 2 and 20 GeV/a. The situation is exacerbated by the inherent fluctuations in the signals. Only an estimate of the energy can be made leading to charge estimates to only the nearest integer. A schematic diagram of the design charge resolution is shown in Figure 6.

The energy dependence of the energy resolution is shown in Figure 7. From threshold (~ 0.4 GeV/a) the rate of change of the scintillation signal in region B decreases with increasing energy leading to a reduction in the energy resolution. As already noted between minimum ionization and the onset of the Freon gas Cerenkov signal the experiment is relatively insensitive to energy. A possible way to fill this gap in a future experiment is with an aerogel Cerenkov radiator (threshold ~ 4 GeV/a). This was considered as an option for a second flight. Beyond ~20 GeV/a the Freon-gas Cerenkov radiator in region C provides energy resolution up to ~ 80 GeV/a. This overlaps the rise in

the gas Cerenkov signal in region B (threshold ~ 70 GeV/a). In turn the region B gas Cerenkov signal overlaps the relativistic rise in the specific energy loss, again providing internal cross-calibration, that extends the energy resolution to several hundred GeV/a. The specific energy loss process has been studied by other groups and a formalism that gives an excellent description of measured high energy data has been developed[14].

The instrument was also designed to provide discrimination against nuclear interactions which will occur for ~ 10% of the events. The Pilot Cerenkov detectors in regions A and C, besides their use as energy sensitive detectors, were used to reject such events. A nuclear interaction will lead to signals in these two regions that deviate from the ratio of the thickness (6 mm in A; 1.5 mm in C) of the Pilot radiators. This ratio is independent of impact parameter. For cosmic rays exceeding ~ 20 GeV/a when the region C Freon-gas Cerenkov signal adds to the Pilot signal, consistency checks with the region B scintillation signal and the Pilot signal from region A can be used as a filter against nuclear interactions.

4. Data Analysis

In this section we overview the analysis techniques; more details are provided in the appendix. Two pre-analysis steps were needed. Firstly, due to the command interference, the photo-tube gains had to be re-balanced in software-- see appendix C. Secondly events striking detector elements: fisheyes in regions A and C and aerials in B had to be identified. Such events were rejected and tallies of their number kept -- see Appendix D.

Due to their geometry regions, A and C are not ideal light integrating chambers: the detected signals have a position dependence. It was necessary to map the distribution of events onto the domed pilot surfaces in these regions -- see section 4.1. Finally in section 4.2 we discuss the determination of the impact parameter from region B.

4.1 Event mapping on region A

The signal amplitude detected from a cosmic ray in regions A and C depends not only on the impact parameter but also on where the cosmic ray strikes the domed Cerenkov radiators in each region. This position dependence is a common problem in charged particle detectors. It is often solved by mapping the events onto the surface and then applying a correction. This is the technique we have used. Due to the spherical geometry of BUGS-4 it is natural to use spherical coordinates: colatitude (0-75 degrees; 0 is at the pole) and longitude.

There is no correlation between the impact parameter determined from timing the difference between the primary and secondary scintillation (GPS) in region B (section 4.2) and the event coordinates in regions A and C. For example a small impact parameter event in region B is not confined to near polar trajectories. The only constraint is that it must strike somewhere on region A, pass close to the central electrode in region B and then strike region C.

We have applied a simple vector model[15] that does not require any *a-priori* decision as to the event location. We map the tracks on to a disc by constructing vectors normalized to a maximum of 100:

$$Vx = (I_3-I_7+(I_2+I_4)\cos(45)-(I_6+I_8)\cos(45))¥(normalization/mean)$$

1.

$$Vy = (I_1-I_5+(I_2+I_8)\cos(45)-(I_4+I_6)\cos(45))¥(normalization/mean)$$

2.

I_1 is the signal in tube pair 1 etc.; see Figure 8. We also constructed a mathematical model of region A. For this model we must relate an arbitrary impact coordinate on the Pilot surfaces in region A to the detected signals in each of the eight tube pairs. Simulations[14] indicate that a useful parameter is the great circle distance (gc) from the event coordinate to the point on the Pilot closest to each tube. A phenomenological model using this parameter was developed. For each randomly selected event coordinate on region A we compute the signal for each tube as:

$$2.29 \neq (1.02e6/(gc_2 + 1.21e4) + 1.71e5/(gc_2 + 1.71e2))$$

3.

The first term models the diffusion of light within the cavity. For large values of gc, (tubes furthest from the event) this term also models the integrating chamber component. The second term represents the direct illumination component. The coefficients have been adjusted to reproduce the observed biggest/mean distribution (see appendix E) and normalized to the average iron signal in p.e. per channel. Adjacent tubes are summed to simulate the experimental data.

The location of each event, in this model, shown in Figure 9a (data) and 9b (simulation), is specified by the Cartesian coordinates V_x, V_y. These plots can be used to identify fisheye hits but the techniques discussed in appendix D are more suitable. The hole in the center of both figures is because there was no Pilot around the probe mount. In Figure 9a (data) it is larger than in Figure 9b (model). Initially we felt this was a deficiency of the model. Several different formulae relating impact coordinate to tube signal were tried; all gave similar results. We believe this dearth of events is caused by optical trapping in the upper hexagon Pilot radiator ring a (Figure 10). Since ring a is approximately circular total internal reflection is more likely than in the more rectangular panels. The reduction in the aperture is small.

To develop more understanding of the response we extend [14] the model to quasi spherical coordinates for the domed Pilot surfaces and compute a longitude variable
$$y = \tan_1(V_y/V_x)$$

4.

and a colatitude variable
$$q = \sin_1 \tilde{I}((V_{x2} + V_{y2})_{-0.5})/r_-$$

5.

N.B. in this convention q=0 is at the pole; r is the radius of the Pilot shell. To verify that these approximate coordinates do give a good description we show q against y in Figure 11a (data) and 11b (simulation). For the y values centered on tube pairs the q variable increases rapidly. However, the mean signal varies smoothly with q -- see Figure 12. This smooth variation is easily corrected by a simple algorithm so that the entire aperture of the instrument can be employed.

The region C signals (not shown) are smaller than the region A signals by the ratio of the thickness of the Pilot: 1.5/6 = 25%. The ballast interference set some region C photo-tube voltages so low that the efficiency for detecting the weakest signals (silicon cosmic rays) is reduced for events striking near the pole of region C. This changes the impact parameter distribution for these species. Hence when comparing the measured impact parameter distribution with theoretical predictions (section 5.1) only iron group events are used.

11

4.2 Determination of the impact parameter

A more detailed discussion of the drift waveform and the atomic processes will be presented elsewhere by Petruzzo et al. [1] (next paper in this journal). Here we discuss how the impact parameter was measured. To determine the impact parameter the time between the primary scintillation (t_rise ~ 50ns) and the secondary GPS must be measured. The rise time (10-90%) of the GPS is impact parameter dependent and over one hundred times slower: ~ 4 m-seconds for small impact parameters; ~ 28 m-seconds for large impact parameters. The same photo-tube base circuit also had to process a gas Cerenkov signal with a rise time < 10 ns. Hence two signals differing by over 2800 fold in their rise time had to be processed by the same photo-multiplier. A custom active FET photo-multiplier base circuit[16] that extracted both these signals from each of the eight photo-multipliers viewing region B was fabricated. The anode signal measured the fast signals: gas Cerenkov and prompt gas scintillation. The eight dynode signals, that had the essentially D.C. response needed for the drift signal, were hardwire summed and integrated with a simple first order active circuit. The integrator output was digitized every 4 m-seconds. A typical drift wave-form is shown in Figure 13a. The decay of the primary signal is controlled by the integrator time constant that was set at 25 m-seconds.

In many drift chambers no drift field is created until a coincident event, defined by other detectors, is registered. For BUGS-4, the flux of troublesome particles was small. The drift voltage was not pulsed. Since the probe was maintained at 3 kV, there was a possibility that a random event could contaminate a coincident event. This could lead to two drifts, or a large random drift overlapping a weak good drift. To provide discrimination against such events the integrator was continually digitized such that 276 m-seconds of pre-trigger waveform were recorded along with each coincidence wave-form.

We now discuss the post-flight wave-forms analysis that was implemented using the code Daphne[17] on a VAXstation 4060. All the 30,000 events analysed could be processed in a few minutes. The background from a-particles and protons striking the photo-cathodes is discussed in appendix E.

The drift processing was performed in two consecutive steps: Stage A and Stage B. The most stringent processing (Stage A) was on the integrated wave-forms since fluctuations that troubled the drift algorithms were more noticeable after de-convolution of the integrator. From Figure 13a it can be seen that a good drift pulse must follow a negative gradient from the primary. The wave-form then rises smoothly with a positive gradient, peaks and decays. The only exceptions are events at small impact parameters that rise before the primary has decayed or decayed very much. Such events are specifically searched for. The maximum extent of the drift wave-form is a constant for all coincident events: electrons must necessarily drift from the chamber perimeter. However, it is not a useful reference for suppressing random events whose wave-forms must terminate at different positions. The statistical fluctuations are too large.

In Stage B the deconvolved wave-forms were analyzed. The deconvolved wave-form from Figure 13a is shown in Figure 13b. Consistency checks were made between the impact parameters determined in both stage A and B.

The impact parameter for events passing both stage A and B processing, was calculated from a fit (see Petruzzo et al [1] relating the measured drift time to the impact parameter. The impact parameter distribution is presented in section 5.1. Raw and corrected signals in regions A and B are presented by Petruzzo et al.[1].

5. Flight Performance of BUGS-4

In this section we present the overall performance of BUGS-4. Firstly we show that the measured impact parameter is in good agreement (section 5.1) with theoretical expectations. We then discuss the charge resolution.

5.1 The measured and predicted impact parameter distribution.

One major design aim of BUGS-4 was to correct the trajectory dependence in all regions from the single measurement of the drift time. To verify that the drift processing routines were performing correctly the aperture factor as a function of impact parameter was calculated. As shown in Figure 14 it is in excellent agreement with the measured impact parameter distribution. The impact parameter was then used to correct the signals in all regions of the detector – see Petruzzo et al.[1].

5.2 The Charge resolution

The majority of the events, due to the geomagnetic cut-off, do not produce a Freon gas Cerenkov signal. To determine the cosmic ray charge we must eliminate the velocity dependence from the specific energy loss and Cerenkov signals. The technique was developed for the Bristol experiment on Ariel 6 and is implemented as:

$$\text{Normalization} ¥ (\text{Scintillation})_x ¥ (\text{Cerenkov})_{(1-x)}$$

6.

The power index (x) is a calculated parameter that is empirically adjusted to optimize the charge spectrum; a value of 0.6 was used. Nuclear interactions are removed using the ratio of the Pilot Cerenkov signals in regions A and C. A simulated charge spectrum is shown in Figure 15a. The data (Figure 15b) has much poorer resolution: $s_z \sim 1.5$ charge units compared with the expected 0.3. We believe the experimental resolution is significantly degraded because of the command interference. This perturbed the photo-multiplier gain balance and we could only re-balance summed pairs of photo-tubes since they were summed before digitization -- see appendix C.

6. Conclusions

Exceptional factors, unrelated to the design have complicated the analysis of the BUGS-4 test flight data. The analysis has overcome these problems sufficiently to show that the BUGS-4 design concept works well. The features in the technical implementation that need further improvement are apparent from the analyzed results. A simple method to map and correct the position dependence of the signals in the two Pilot Cerenkov radiators allows the whole aperture factor of 4.5 $m_2 sr$ to be exploited. A single measurement of the drift time allows all the path length dependence in the multi-element instrument to be corrected.

Several innovative technologies have been developed and successfully deployed. Most notable was the large spherical drift chamber which incorporated several new techniques. These include the ceramic drift probe, the region B aerials and the active FET photo-tube bases.

No serious background problems were found. The pre-flight and flight fluctuations on the drift signals are indistinguishable indicating that the copious flux of a-particles and

13

protons do not cause a significant background. Also encouraging is that there are no serious problems from secondary hits on the region B aerials or photo-tubes during the drift measurement, as predicted by approximate pre-flight calculations, even though the drift wave-form digitizer operated for over 1 ms following a coincident trigger.

The flight has provided crucial information to guide the design and construction of a future instrument. In a BUGS-5 instrument designed to sample lighter species to boron (Z=5) it will be necessary to immunize against hits on the detectors in the central region during drift wave-form measurement. As we have mentioned this is easily achieved. It will also be advantageous to extend the dynamic range for the digitization of the fast signals in region B. Again this is easily done.

In summary and conclusion the design provides a relatively inexpensive means to study the charge spectrum of the primary galactic cosmic rays over a wide energy range.

7.   Acknowledgments

8.   Appendices

8.1   Appendix A: The mechanical construction of BUGS-4

The mechanical construction of BUGS-4 was a considerable challenge due to the very tight tolerance required in the spherical drift chamber coupled with strict weight limits. The entire mechanical construction was performed at the University of Bristol (UK).

The tolerance required for the inner pressure vessel was (0.0025 m). This could only be achieved by spinning. However, no aluminum sheets of suitable dimensions were available. A commercial fabrication facility was employed to weld two sheets to the appropriate size but their welds failed during the spinning process. Technical staff (Brine and Head, 1982[19] at the H. H. Wills Physical laboratory in Bristol perfected a welding technique that created welds that were essentially indistinguishable from the parent S1B material: minimum 99.5 % pure aluminum; maximum 0.05% Cu, 0.3% Si, 0.4% Fe, 0.05% Mn, 0.1% Zn. Four welded sheets, to give two spares, were spun on a specially constructed cast iron jig. These sections extended to a polar angle of 75 degrees, with a polar thickness of 0.47 cm that reduced to 0.31 cm at 75 degrees. The top hemisphere was equipped with a polar mount to accept the ceramic probe that was installed in region B -- see section 3.3. These two sections were then welded to a flange using a custom motorized assembly.

A belly band section was constructed from spun sections and equipped with eight large port holes to accommodate the eight photo-multiplier tubes; orifice for pumping, pressure transducers and sources were also provided -- see Figure 16. Flanges, with an 'o' ring groove, were welded to the belly band in a form to match the spun sections so as to create a vacuum seal when the assemblies were bolted together. To the top and bottom joint, large flanges that contained sixteen ports for photo-tubes that viewed regions A and C were added (see Figure 16). The inner section of the belly band was painted with a reflective coating of $BaSO_4$. The background scintillation from $BaSO_4$, that would swamp the gas Cerenkov signal, precluded its use for the remainder of region B. The inner surfaces were processed to enhance the reflectivity and to produce a diffuse rather than specular reflector. This was achieved by bead-blasting (to create a spherically indented surface) and then chemically brightening for three minutes in a PHOSBRYTE 156 solution: a chemical agent based on phosphoric and sulphuric acid. Between production and flight the central chamber was stored, due to administrative factors, for over ten years. Although it was necessary to clean the surfaces with alcohol, the reflectivity, as checked with a precision reflectometer, was unchanged from the production condition.

The outer pressure vessel was constructed from spun aluminum panels of thickness 3.5 mm. Since they had to tolerate greater pressures than the central chamber they were formed from a stronger aluminum alloy: grade N6; maximum 4.5-5.5% Mg, 0.1% Cu, 0.3% Si, 0.4% Fe, 0.05% Mn, 0.1% Zn; remainder Al. The spun sections were welded together to form two outer dome surfaces. Flanges were welded to the perimeters. An outer belly band section (see Figure 16) was fabricated from spun sections, and provided with eight large access ports. This was welded to a flange that mated with the two outer domes. These assemblies were then attached, so as to form a vacuum seal, to the flanges that extended from the central region (see Figure 16). Hence three regions A, B, C and the equatorial space D were constructed.

Regions B and C were independently isolated from all other regions. Before flight region C was filled by adding Freon-gas slowly to the bottom, so that the air was vented by displacement through a valved pipe at the top of region C that passed through region D to a Freon-recovery facility. The equatorial region D was common to region A. Regions A, B and C although isolated from each other had to remain at the same pressure to within ~ 1 lb./inch2. The assembly was pressure tested in Bristol dock. The inner surfaces of regions A and C were coated with $BaSO_4$. This coating deteriorated significantly in storage and was completely replaced after the detector was shipped to Huntsville.

8.2 Appendix B: The flight electronics

BUGS-4 contained 16 photo-multipliers in regions A and C along with 8 in region B. Each of these 40 photo-multipliers was supplied with an independent, remotely controlled, high voltage supply. An additional commandable voltage supply was used to control the probe voltage.

To reduce the complexity of the digitization electronics the signals from the photo-multipliers in regions A and C, which were mechanically grouped in pairs, were also summed in pairs before digitization. Due to the dynamic range of the signals in these regions the anode signal was split and one component fed directly to a charge sensitive LeCroy 2249 ADC. The second component was fed to a custom built pre-amplifier, based around a LeCroy HQV810 chip, then to the LeCroy 2249 ADC. Hence 32 ADC channels were required to digitize the signals in regions A and C.

Of the 40 photo-multiplier tubes flown on BUGS-4 only one (tube B8) failed to deliver any useful information. The direct feeds from tubes A3, C4 and C6 failed.

However as the amplified signal was present the fault was not with the photo-multiplier. Since the signals fed to adjacent channels of the ADC functioned we believe the problem was connected with the cabling.

The instrument coincidence acceptance was defined from a remote controllable discriminator that was fed from the 16 dynode signals in region A and eight paired dynode signals in C.

Each photo tube in region B was required to sample both fast (t_rise ~10ns) and slow (t_rise ~24 m-seconds) signals. To accomplish these requirements each tube was equipped with an active[13] FET base. The anode signals from these bases were fed to LeCroy 2249 ADC. In addition a sum of the anode signals was fed to a delay line sampler such that 12 samples, each separated by 10 ns, of the prompt region B signals were collected. These data would have been used to recover the gas Cerenkov signal from the composite with the prompt gas scintillation. -- see section 3.3. The dynode signals, which had essentially D.C. response, were summed and integrated with a first order active integrator. This signal was sampled as described in section 4.2.

The LeCroy ADCs were read by a CAMAC system. The data was then shifted through a VME system based around a Motorola 68030 processor before radio transmission to the ground station at Ft. Sumner, New Mexico.

8.3 Appendix C: Gain matching

Due to the interference from the first ballast command that took place shortly after launch the photo-tube gains had to be re-matched. The first step in this process was to look at the digitized spectrum from each ADC and to apply crude gain factors to align the overall shapes. The sum of the region B tubes then had sufficient resolution to define a iron group. Spectra for each channel, gated on this iron group, were examined and corrections to the gain factors made. This procedure was repeated several times as our understanding of these data improved. Gain mis-matches resulting from each tube in a pair (regions A and C) having different gains could not be corrected. This is a practical limitation which we believe significantly degrades the charge resolution.

To check for a time dependence the iron gated signals in 1,500 event intervals were examined. Although the distributions are broadened by the p.e. statistics (~200 p.e. per tube pair), the colatitude dependence and the non-saturated Cerenkov distribution the centroids can be read with some accuracy. These did not vary by more than ~10% over the first 30,000 events.

The factors required to re-match the gains, Table 2, show the severity of the interference.

8.4 Appendix D: Events that strike photo-tubes aerials or fisheyes

In this appendix we discuss events that strike the photo-tube based detection system during measurement of the prompt signals. Since cosmic rays illuminate the entire instrument, it is inevitable that some will strike the fish eyes viewing regions A and C; others will hit the aerials viewing region B. A few will interact with detectors in more than one region. Another contribution is knock-on electrons from a cosmic ray passing close by a photo-tube.

In all cases the event is characterized by a large signal in the polluted channel and a small mean signal as was noted on BUGS-2B[20]. A suitable parameter to identify these

16

events is the quotient of the biggest to mean (B/M). In Figure 17 we show a plot of 100¥log(10¥mean) against 10¥(B/M) (ordinate) in region A. Region C behaved like region A. The events that strike the fisheyes (B/M _ 4) are cleanly separated indicating that the fisheyes were well coupled to the photo-multipliers.

Signals that exceeded the ADC dynamic range were recorded as a constant K (typically 1955 for the 2048 channel ADC used). The B/M value for these events is 8¥K/(K + D); D is the contribution of the other tube pairs. For events that are dominated by one tube B/M tends to 8. For other events D controls the expression. This is the origin of the weak loci of the form (B/M)= (log(mean))-1 seen in Figure 17.

In Figure 18 we show a B/M plot for region B. Here the aerial events are less cleanly separated and we choose to use a B/M gate of < 2.5 to select good events. The smaller B/M variation in region B compared with region A shows that the region B surface treatments (see Appendix A) produced an approximate integrating sphere response. Region A, by contrast, has a strong colatitude dependence.

The number of events, including overflowed events with B/M > 4 (regions A and C) ; B/M > 2.5 (region B), are compared with BUGS-2B19, a similar instrument to BUGS-4, in Table 3.

As expected there is a large imbalance in the region A and C fisheye hit yields that are attributable to the failure of two direct channels in region C. The overflows in each ADC are given in Table 4. In region A, where only one direct signal failed, the overflow rate is small. There are a large number of overflows in region B. In a future experiment it would be advantageous to split the region B anode signal in a similar way to region A (see appendix B), but instead of amplification one channel would be attenuated through, say, a passive resistor network.

8.5 Appendix E: Drift wave-form processing

Although protons and a-particles transversing region B produce insignificant gas scintillation signals they may masquerade as a prompt gas scintillation signal if they strike a photo-cathode: the tubes were hard wire summed such that a large signal in one is indistinguishable from a sum of smaller signals detected in all the tubes. There is an appreciable probability for direct hits on the photo-cathodes.

The aperture factor[21] for a plane surface of area A is 2¥p¥A which for the seven active photo-cathodes (diameter 5 inches) in region B is 0.56 m2sr. The fluxes of a-particles and protons, at a rigidity of 4.1 GV, are ~ 137 and ~ 758 m2sr/s. These fluxes were measured at the 1987 solar minimum and are therefore upper limits. The number of expected hits on the photo-cathodes during the drift wave-form processing (276 m-seconds of pre-trigger; 748 m-seconds of post trigger) is 895¥0.56¥(1024e-6) = 0.51. Hence an a-particles or proton will strike at least one photo-cathode during ~ half of the drift wave-form measurements. There will also be a component from protons and a-particles that have long path lengths in the aerials.

Due to the large rate of such events the pre-trigger and post-trigger processing was performed differently. Since nothing occurring in the pre-trigger can be related to a genuine coincident event any signals in the pre-trigger that exceeded the average by 30% lead to the event being rejected. Since such events are random this does not bias the impact parameter measurement. However in the post-trigger portion of the wave-form signals with a fast rising edge (the characteristic of prompt primary events – see Figure 13a- were ignored since most came from hits on the photo-cathodes. The algorithms also looked for and

rejected multiple drift wave-forms. A final check came from the gas gain: the ratio of the drift area to the primary scintillation which is a constant for good events.

The event processing efficiency was 87%. Most of the rejections were for multiple drifts and a signal in the pre-trigger. The number of pre-trigger events caused by direct hits on the photo-tube cathodes can be reduced by demanding that at least two tubes detect an event using a simple threshold coincidence circuit. Such techniques will be particularly important in a new instrument designed to sample lighter species to boron. The Cerenkov signal from an a-particle striking a region B aerial (total aperture 3.11 m2sr) may be mistaken for a boron cosmic ray. Demanding a coincidence of at least two tubes during measurement of the drift wave-form will also suppress such events.

The number of multiple drift events can be reduced by decreasing the drift time. The simplest way to do this is to increase the drift field either by changing the central electrode diameter or by improving the probe so that it can tolerate higher voltages. However, this is not attractive as the drift time decreases only as the square root of the probe voltage. Other gas fills with different drift properties can be used. A mixture with xenon has advantages including a substantial increase in optical output. Some tests with xenon in a test chamber have been made. We hope to do further development work.

References

1.   J.J. Petruzzo III, A.E. Smith, J.C. Gregory, R.W. Austin, J.H. Derrickson, T.A. Parnell, M.R.W. Masheder, P.H. Fowler, C. Thoburn, "A 1-meter radius spherical electron drift chamber for the measurement of relativistic heavy nuclei," *Nucl. Instrum. Meth. Phys. Res.* 402 (1) (1998) 123-138.

2.   M. Garcia-Munoz, J.A. Simpson, T.G. Guzin, J.P. Wefel and S.H. Margolic, "Cosmic-ray propagation in the galaxy and in the heliosphere: the path length distribution at lower energy," *APJ Supplement Series* 64 (1987) 269.

3.   D. Muller, S.P. Swordy, P. Meyer, J. L'Heureux, and J.M. Grunsfield, "Energy spectra and composition of primary cosmic rays, APJ 374 (1991) 356.

4.   Ichimura et al., "Observation of heavy cosmic-ray primaries over the wide energy range from ~ 100 GeV/particle to ~ 100 TeV/particle: Is the celebrate "knee" actually so prominent?" *Phys. Rev.* D48 (1993) 1949.

5.   S.P. Swordy, J.L'Heureux, P. Meyer and D. Muller, "Elemental abundance in the local cosmic rays at high energies," *APJ* 403 (1993) 658.

6.   J.J. Englemann, P. Ferrando, A. Soutoul, P. Goret, E. Juliusson, L. Koch-Miramond, N. Lund, P. Masse, B. Peters, N. Petrou and I.L. Rasmussen, Charge composition and energy spectra of cosmic-ray nuclei for elements from Be to Ni: Results from HEAO-3-C2," *Astron and Astrophys.* 233 (1990) 96.

7.   W.R. Binns, T.L. Garrard, M.H. Israel, M.D. Jones, M.P. Kamionkowski, J. Klarmann, E.C. Stone, and C.J. Waddington, "Cosmic-ray energy spectra between 10 and several hundred GeV per atomic mass unit for elements from 18Ar to 28Ni: Results from HEAO 3," *APJ* 324 (1988) 1106.

8.   S.P. Swordy, J. Grunsfeld, J.L'Heureux, P. Meyer, D. Muller and K. Tang, "Observation of transition radiation from relativistic heavy nuclei," Phys. Rev. D42 (1990) 3197.

9.   S.P. Ahlen, B.G. Cartwright, and G. Tarle, "Near threshold response of a wave-shifted Cerenkov radiator to heavy ions," *Nucl. Instr. and Meth.*, 136 (1976) 235.

10.   G. Tarle, S.P. Ahlen, and B.G. Cartwright, "Cosmic ray isotope abundance from chromium to nickel," *Ap. J.*, 230 (1979) 607.

11. P.H. Fowler, A.M. Gray, M.R.W. Masheder, R.T. Moses, R.N.F. Walker and A. Worley, "Design and performance in orbit of the Bristol Cosmic Ray Detector on the Ariel VI satellite," *Nucl. Instr. and Meth.*, A275 (1989) 175.

12. This innovation followed from an informal suggestion by Georges Charpak who received a Nobel prize 91992) for his work on gas proportional counters.

13. C. Alsop, "A large detector for cosmic ray abundance and energy measurement," PhD thesis, Univ. of Bristol, Great Britain (1982), unpublished.

14. W.W.M. Allison and J.H. Cobb, "Relativistic charged particle identification by energy loss," *Ann. Rev. Nucl. Part. Sci.* 30 (1980) 253.

15. M. Grande, "A detector for cosmic ray charge and energy measurement," PhD thesis, Univ. of Bristol (1982), BS8 1TL, U.K.

16. M.R.W. Masheder, R.W. Austin, and T.P. Fagan, "A FET Photo-multiplier base," To be submitted to NIM. Those interested should contact Dr. Masheder at the Department of Physics, University of Bristol, BS8 1TL, United Kingdom.

17. Tom Moog, "Experimenter's Guide: Daphne data acquisition system," Physics Division, Argonne National Laboratory, 9700 South Cass Avenue, Argonne, Illinois, (1988).

18. Present address, Polhode Inc.; Internet: moog@polhode.com.

19. K. Brine and R. Head, "Pulsed MIG welding Aluminum for hemisphere spinning," *Metal Construction* 183 (1982).

20. J.G. Phillips, "The detection of ultra-heavy cosmic rays using a large gas scintillation-Cerenkov detector," Ph.D. thesis, Univ. of Bristol, U.K. (1980), unpublished.

21. J.D. Sullivan, "Geometrical factor and directional response of single and multi-element particle telescopes," *Nucl. Instr. and Meth.* 95 (1990) 5.

Table Captions:

Table 1 Comparison of the parameters of BUGS-4 with those of three contemporary active instruments.

Table 2 The gain factor corrections used to correct the signals after the interference from the ballast commands.

Table 3 Comparison of the number of events that struck fisheyes or aerials in BUGS-4 with the same quantities for a predecessor instrument BUGS-2 - - see text for details.

Table 4 The number of events that overflowed the ADC in regions A, B and C of BUGS-4.

Table 1

Instrument	Aperture (m^2sr)	Energy range GeV/a	Charge range	Thickness (g/cm^2)	Platform	Observational Exposure[1] (m^2sr days)
HEAO-3-C2	0.07^2	$1 \leq E \leq 35$	$4 \leq Z \leq 28$	16	Satellite	33.7
HEAO-3-HNE	5.9^3	$10 \leq E \leq 600$	$Z \geq 18$	3.74^4	Satellite	~365
CRN	0.9^5	$4 \leq E \leq 1000^6$	$5 \leq Z \leq 28$	5	Shuttle	1.93^7
BUGS-4	4.5	$1 \leq E \leq 650$	$8 \leq Z \leq 28$	~3.5^8	Balloon	0.19

[1] Analyzed data

[2] For each direction of propagation.

[3] This is the sum made up from various classes of events

[4] This includes the mass before the instrument and between the two sets of ionization chambers.

[5] The instrument had a design aperture of $5m^2$sr but various restrictions meant that only $0.9 \ m^2$sr was used.

[6] The energy sensitivity range extends beyond 1 TeV but this has not been exploited due to insufficient exposure.

[7] The aperture factor is species dependent. This is the quoted value for iron nuclei.

[8] In addition, for a balloon exposure, there are 3-5 g/cm^2 of residual atmosphere

Table 2

Paired tubes		Single tubes		Paired tubes	
A1	1.224	B1	0.606	C1	1.388
A2	0.453	B2	0.897	C2	0.718
A3	0.753	B3	1.830	C3	1.153
A4	0.804	B4	1.222	C4	0.539
A5	0.883	B5	0.596	C5	1.846
A6	0.743	B6	0.657	C6	0.936
A7	0.794	B7	1.248	C7	0.871
A8	0.360	B8	0.0 channel failed	C8	0.643

Table 3

BUGS-4	Number	% of events	BUGS-2B	
Fisheye in A	1081	3.6%	1627	3.74%
Fisheye in B	2440	8.13%	2537	5.83%
Fisheye in C	2970	9.9%	1614	3.71%

Table 4

A1	35	B1	555	C1	30
A2	79	B2	334	C2	74
A3[1]	521	B3	291	C3	66
A4	38	B4	246	C4[1]	2010
A5	39	B5	438	C5	29
A6	58	B6	378	C6[1]	1065
A7	62	B7	376	C7	71
A8	82	B8	channel failed	C8	243

---

[1] Only an amplified channel was available. The direct signal failed.

Figure captions

Figure 1 A schematic diagram of the BUGS-4 instrument.

Figure 2 A schematic diagram of the signals in each region of BUGS-4.

Figure 3 The relation between the cosmic ray trajectory and the impact parameter in regions A and B. Region A has been drawn oversized for clarity.

Figure 4 A schematic diagram of the optical aerials used in region B.

Figure 5 The time structure of the gas Cerenkov and gas scintillation signals in region B.

Figure 6 The design charge resolution at impact parameters of 0.5 and 0.9.

Figure 7 The design energy resolution.

Figure 8 A schematic plan view of region A showing the algorithms for the Grande model. I1 is the signal in tube pair 1 etc. -- see text for more details.

Figure 9a The mapping of experimental data on to region A using the Grande model.

Figure 9b Simulated data mapped on to region A using the Grande model.

Figure 10 Schematic plan view showing the Pilot tessellation structure in region A.

Figure 11a The distribution of experimental data in region A in terms of the Grande model longitude (Psi) and Grande model colatitude (Theta). The Grande model colatitude exceeds the physical instrument colatitude by ~ 20%.

Figure 11b The distribution of simulated data in region A in terms of the Grande model colatitude (Theta) and longitude (Psi).

Figure 12 The calculated variation of the mean signal with the Grande model colatitude.

Figure 13a A typical measured drift wave form.

Figure 13b The same wave form as Figure 13a but after deconvolution of the integrator -- see text for more details.

Figure 14 A comparison between the measured and calculated (dashed line) impact parameter distributions.

Figures 15a Simulation of the expected charge spectrum.

Figure 15b The measured charge spectrum.

Figure 16 A schematic diagram showing the mechanical construction of BUGS-4.

Figure 17 A plot of 100×LOG(10×(mean signal)) against 10×((Biggest signal)/(mean signal)) in region A.

Figure 18 A plot of 100×LOG(10×(mean signal)) against 10×((Biggest signal)/(mean signal)) in region B.
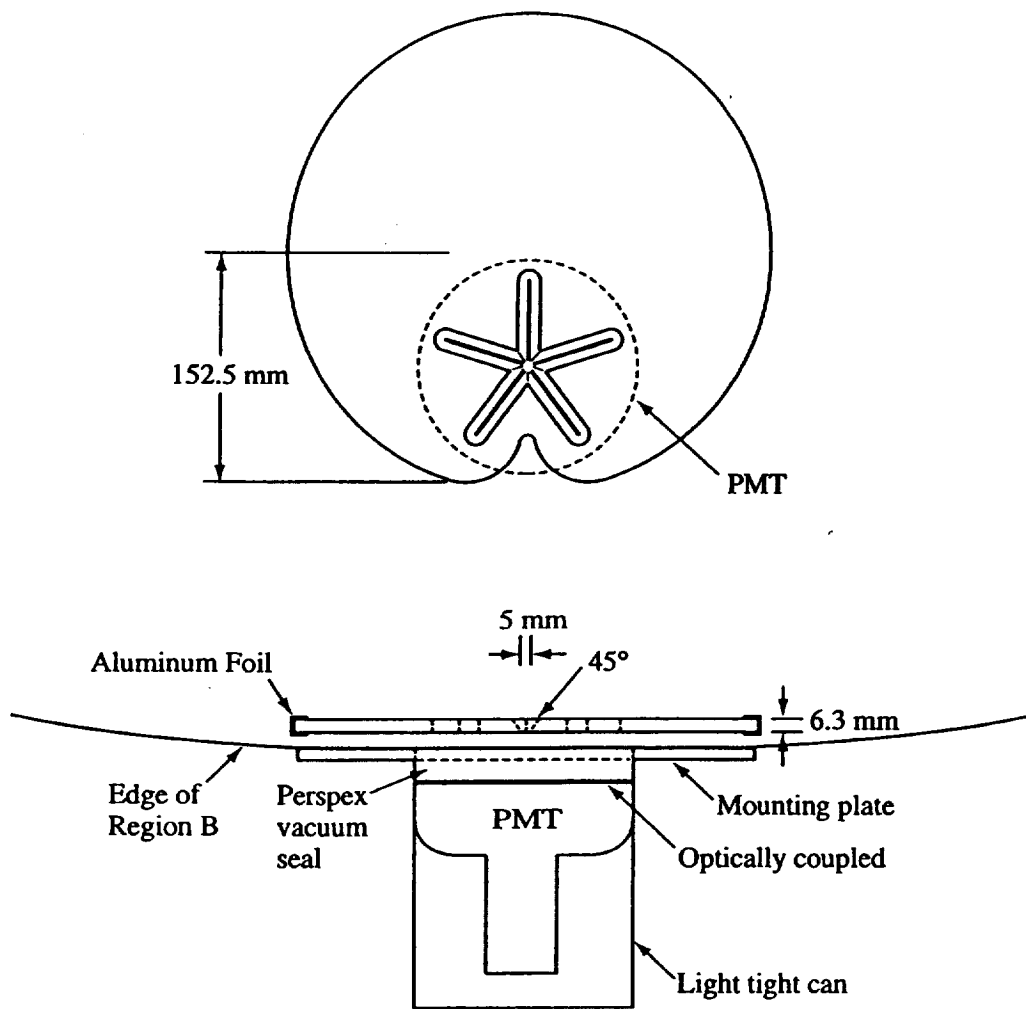
Figure 1

5-23687

Figure 2

Figure 3

Illustrative
Cosmic Ray
Track

5-23766

152.5 mm

PMT

5 mm

45°

6.3 mm

Aluminum Foil

Edge of
Region B

Perspex
vacuum
seal

PMT

Mounting plate

Optically coupled

Light tight can
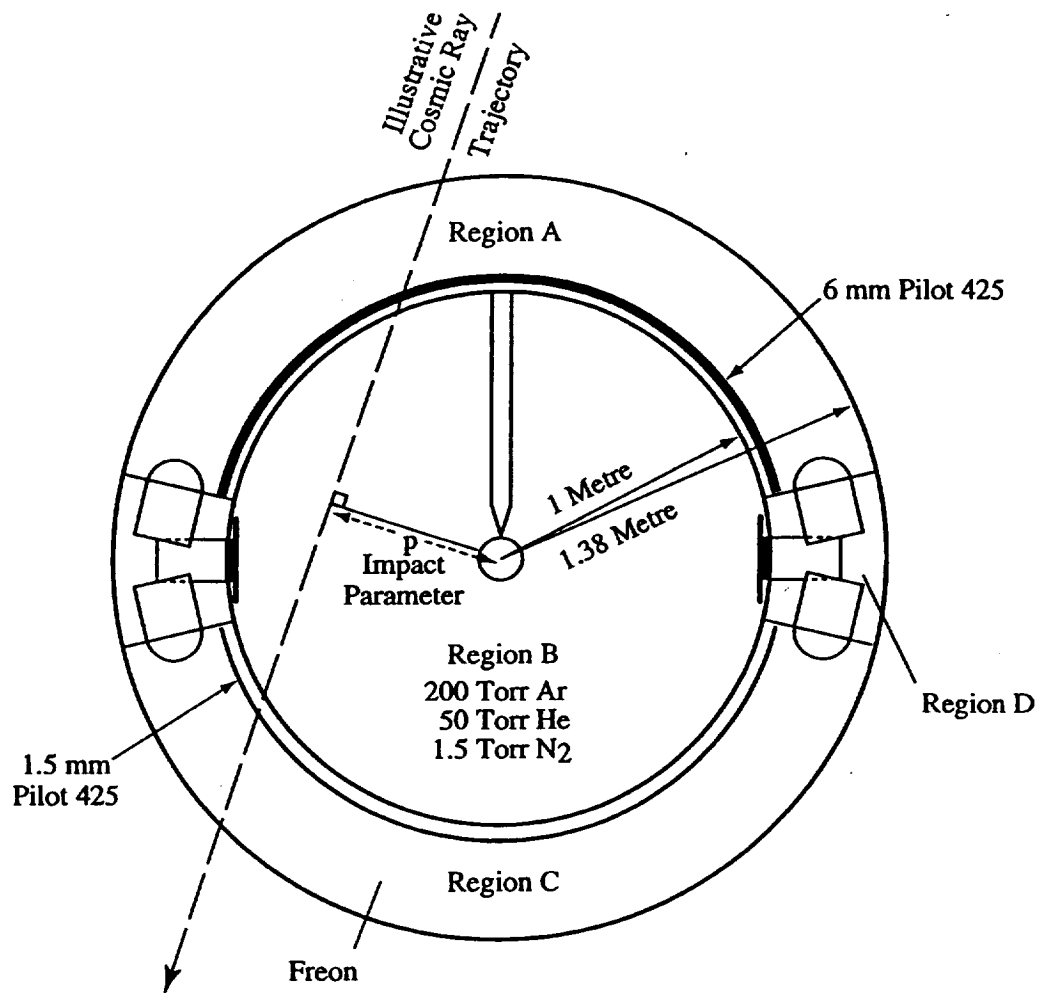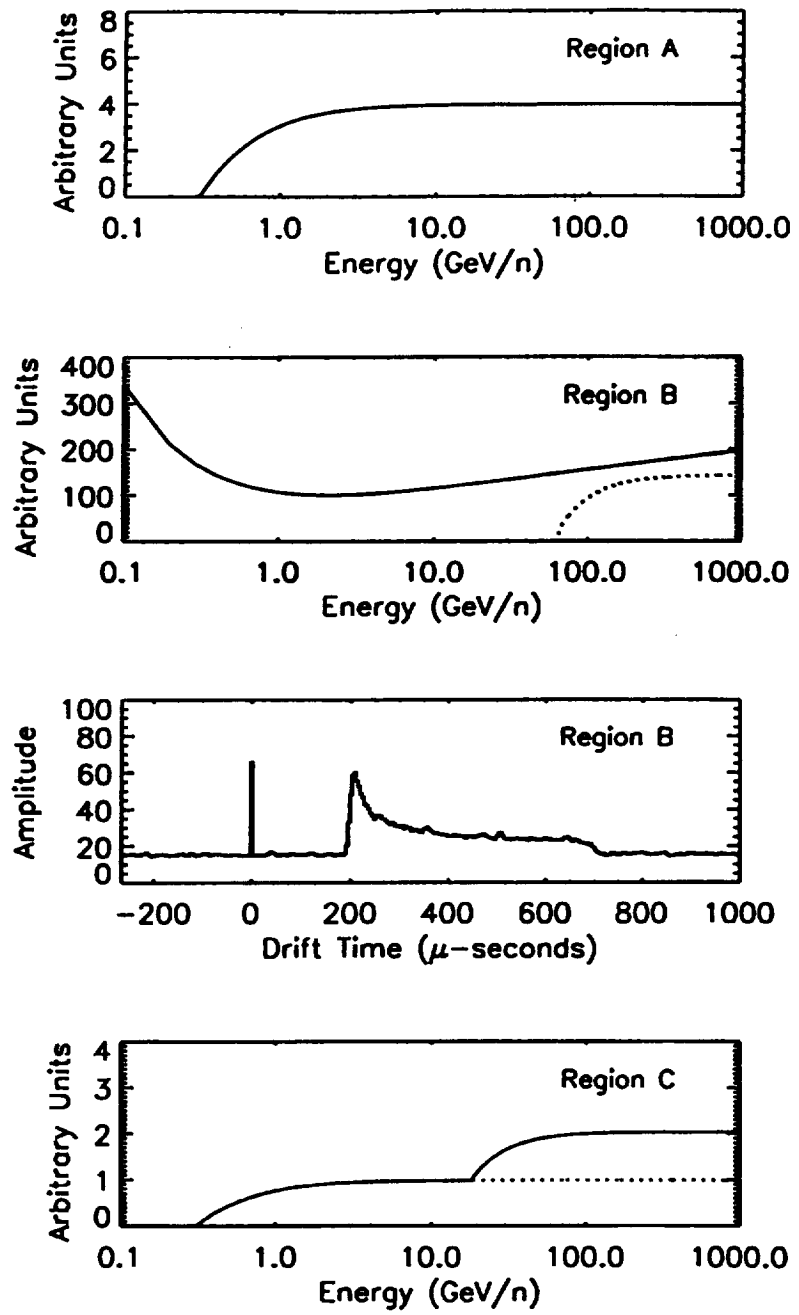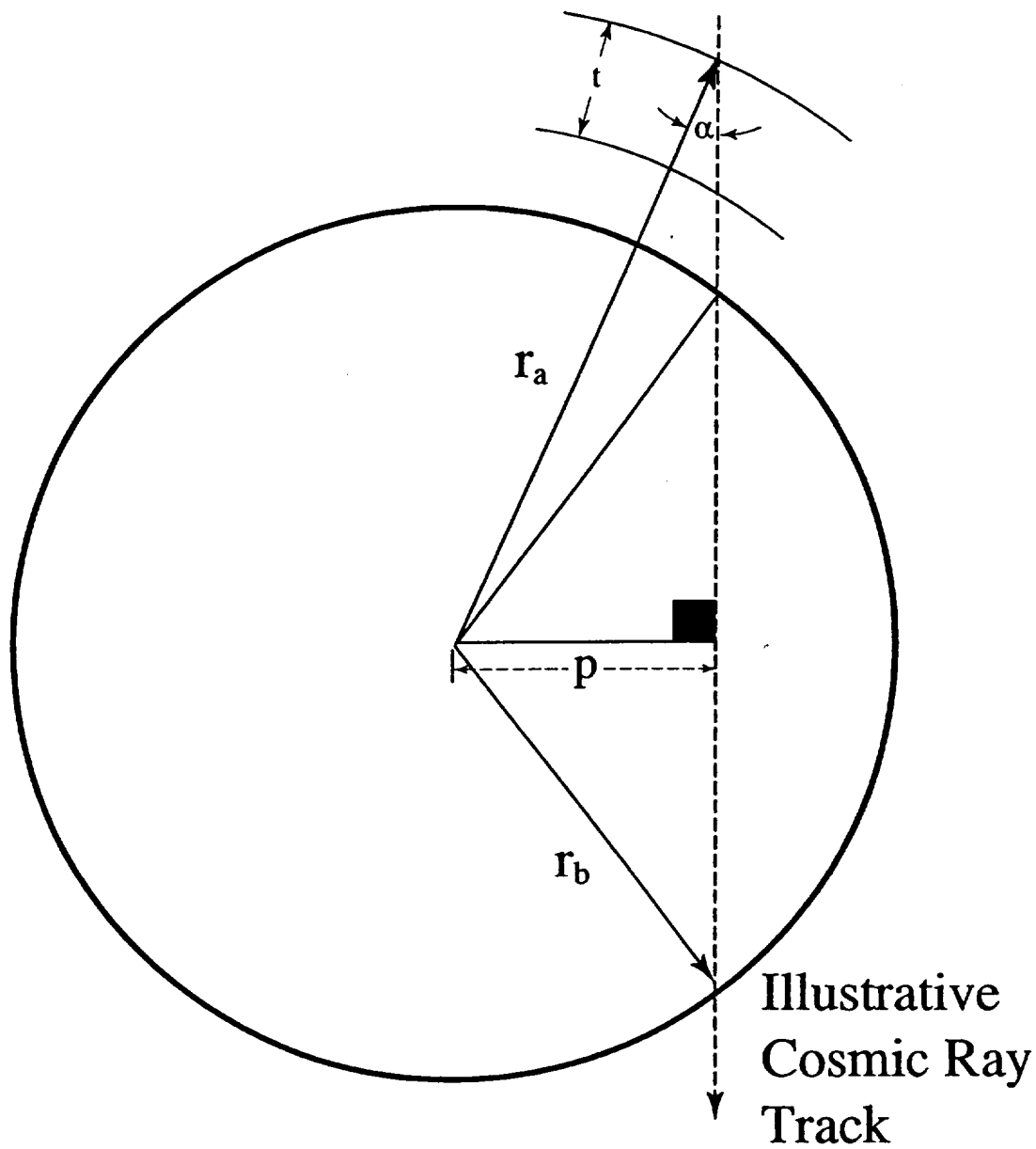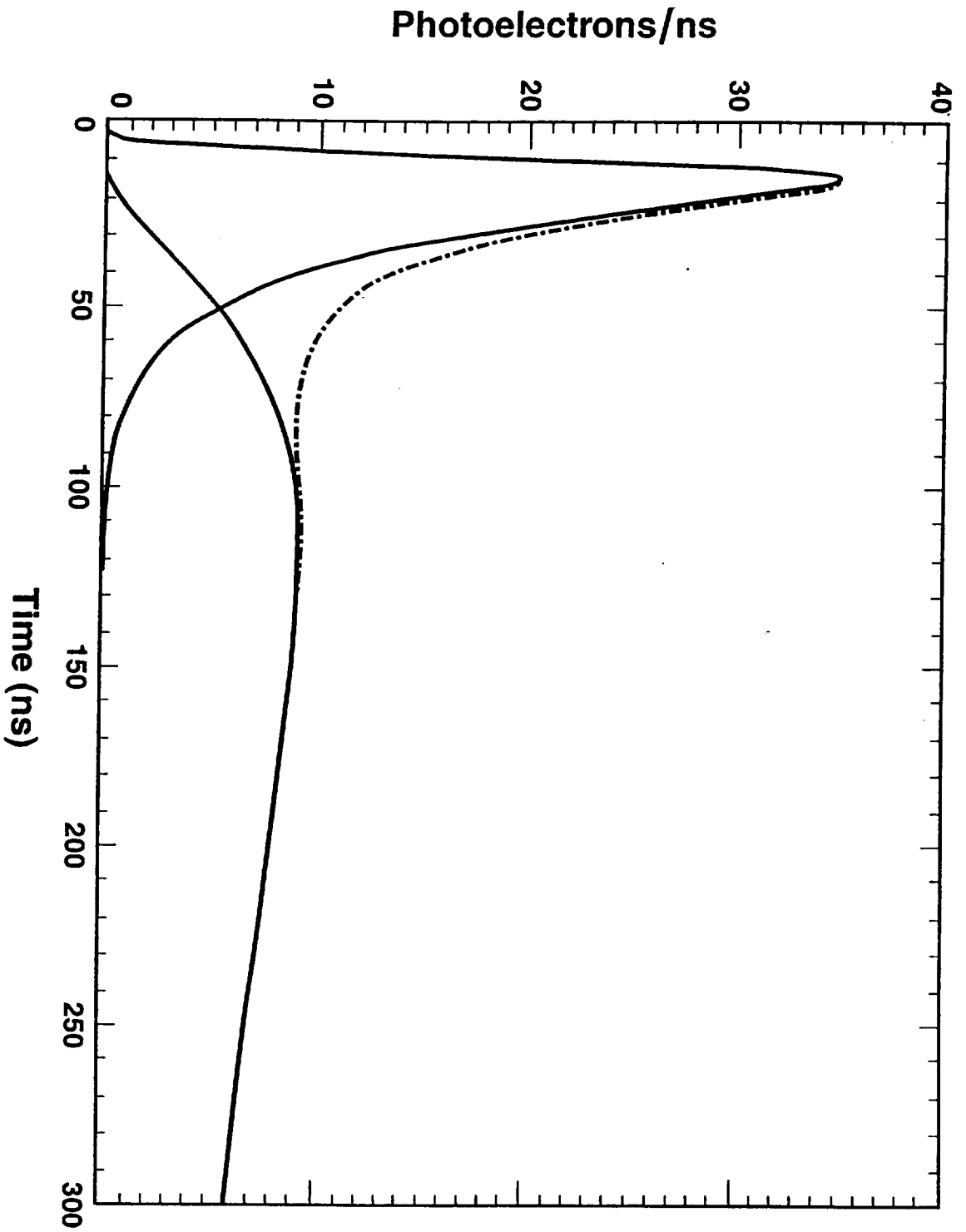
Figure 4

Figure 5

Figure 6

Figure 7

5-30748
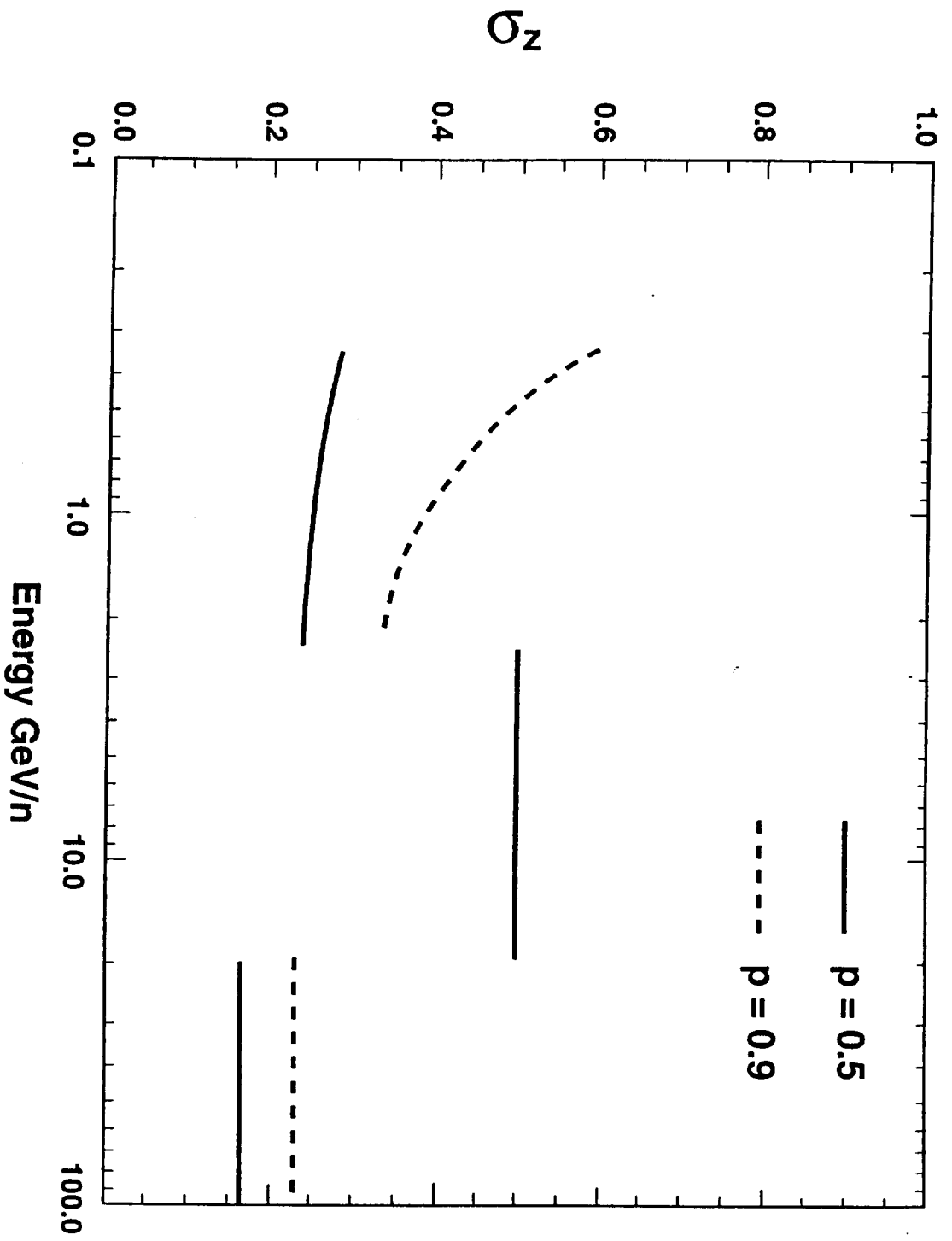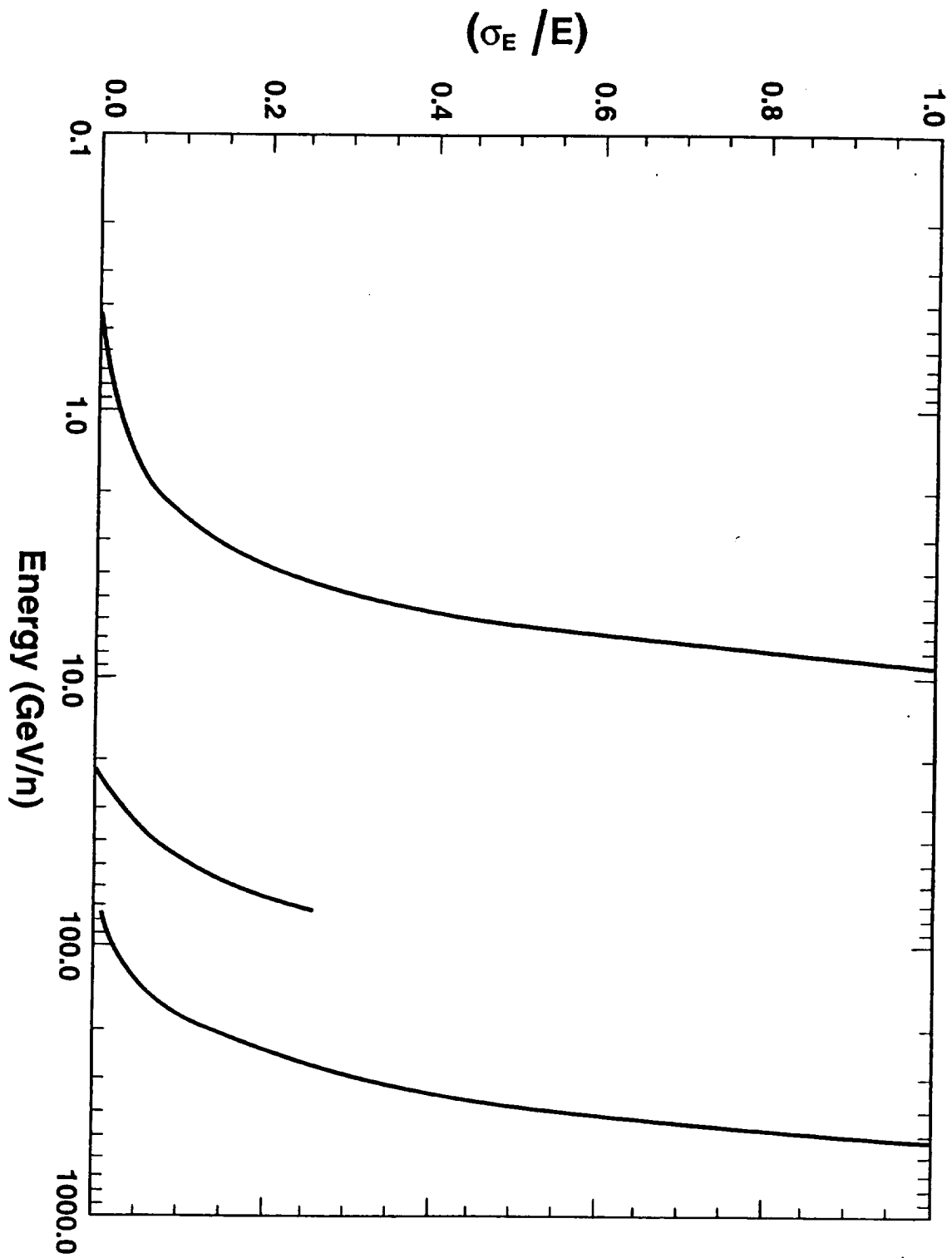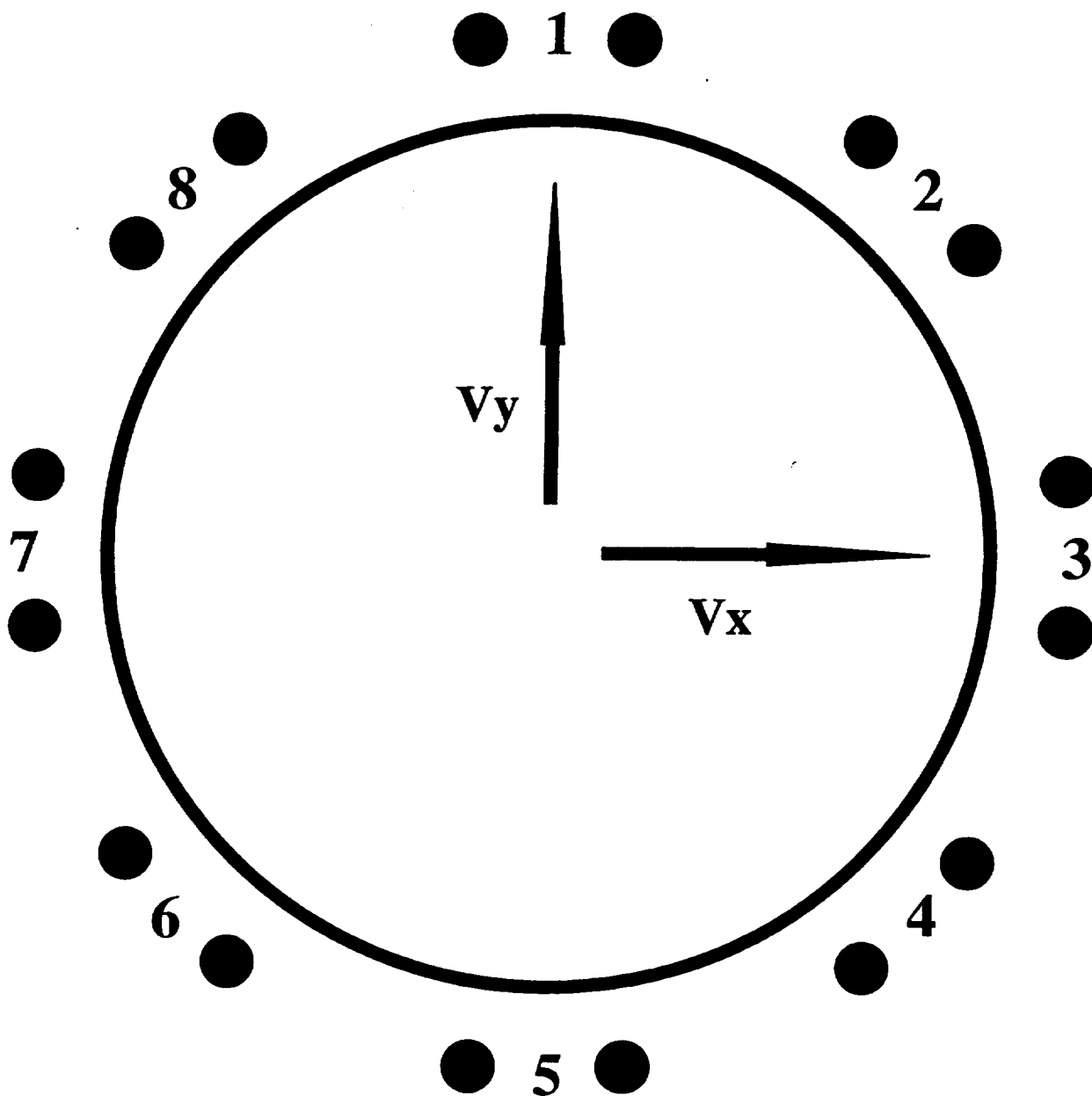
$$Vx = I3 - I7 + (I2 + I4)\cos(45) - (I6 + I8)\cos(45)$$

$$Vy = I1 - I5 + (I2 + I8)\cos(45) - (I4 + I6)\cos(45)$$

Figure 8

Figure 9a

Figure 9b

α β γ δ

One of the
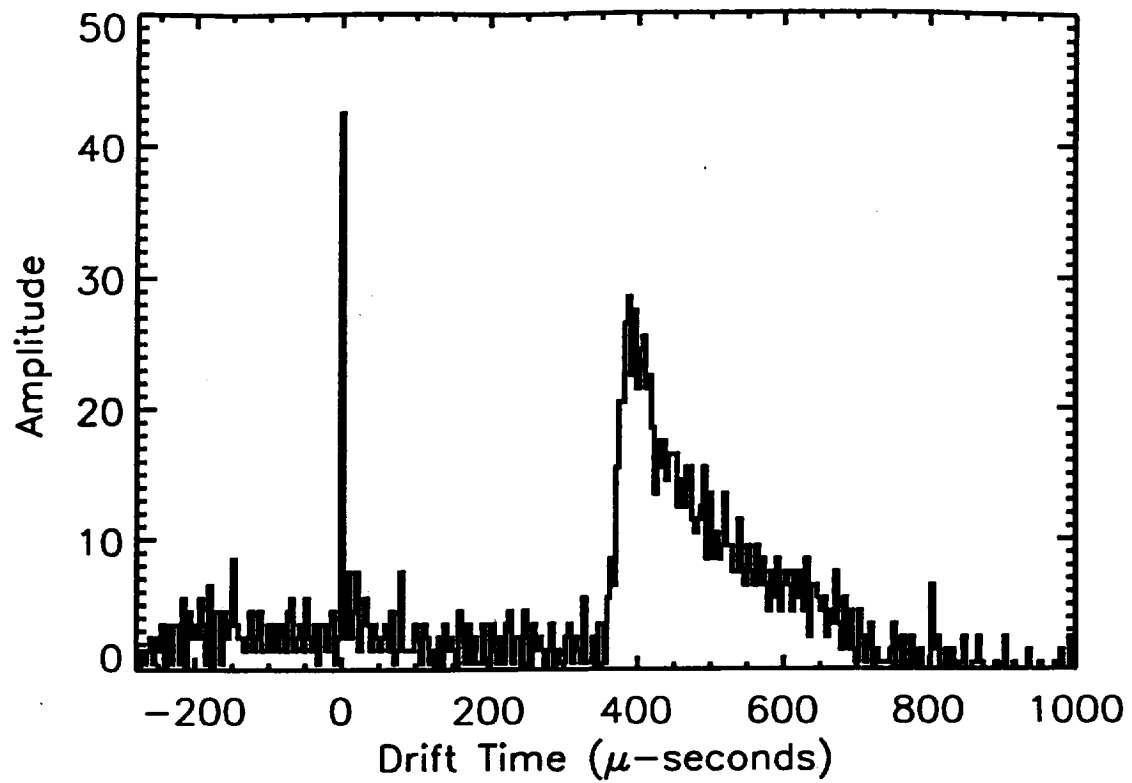16 fisheye lens
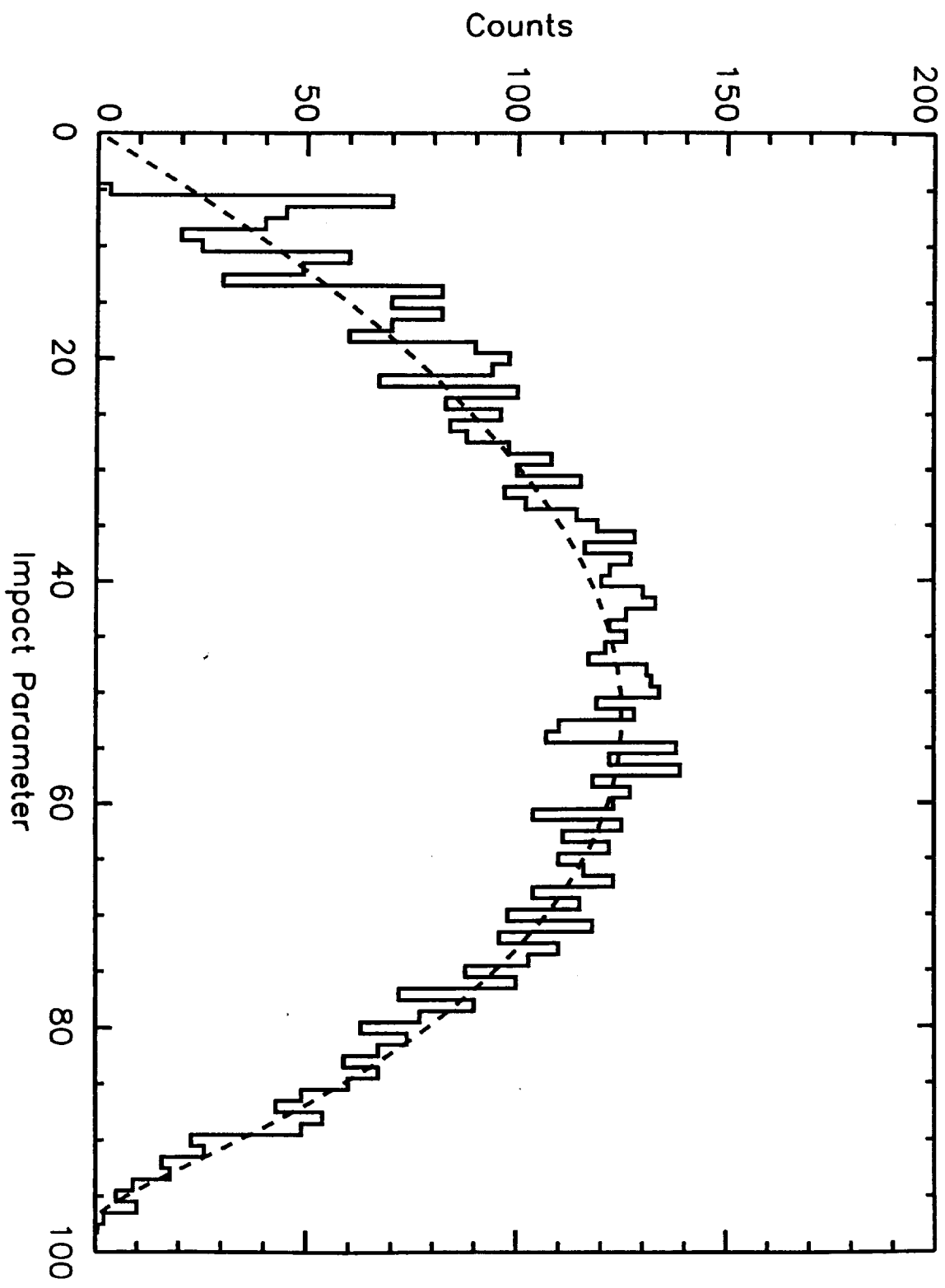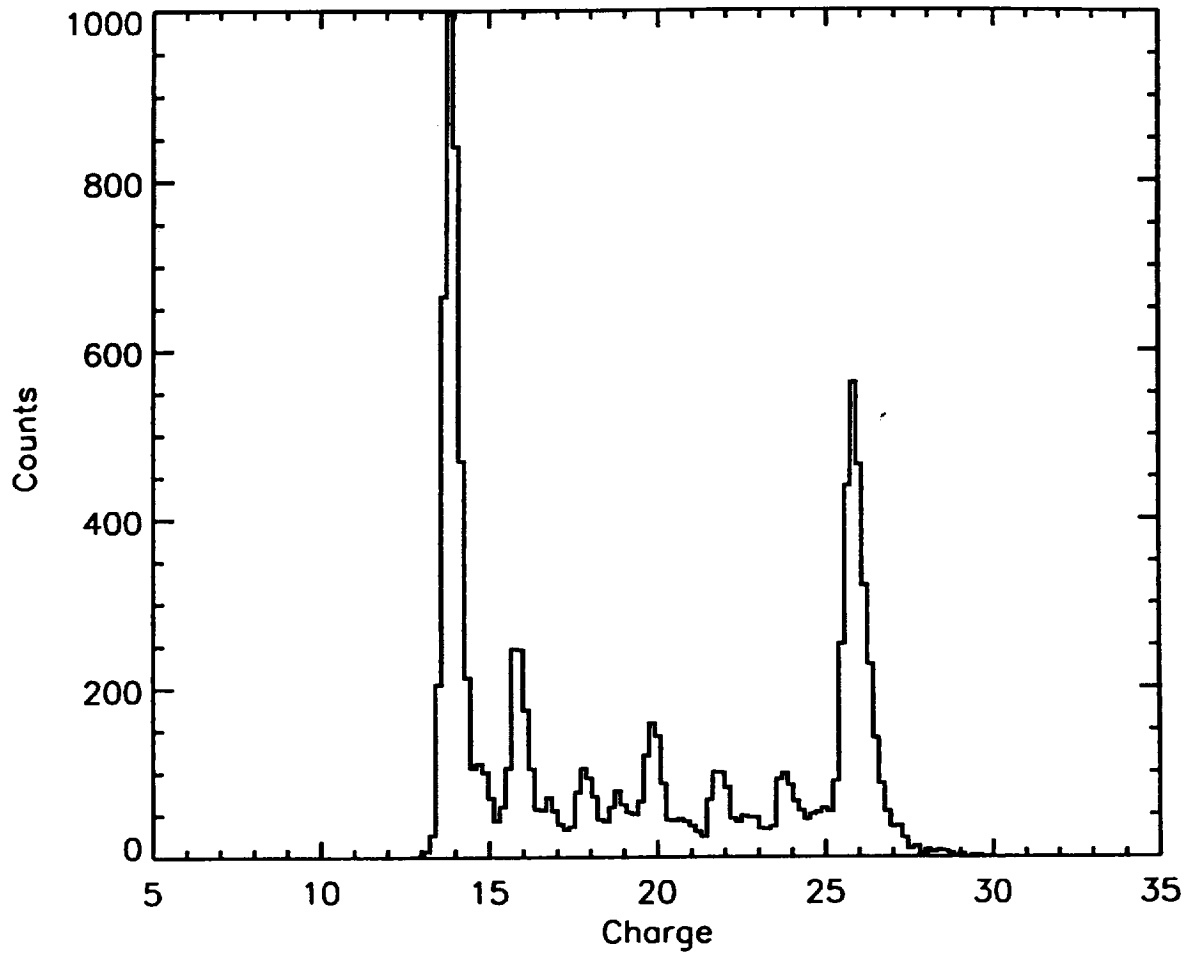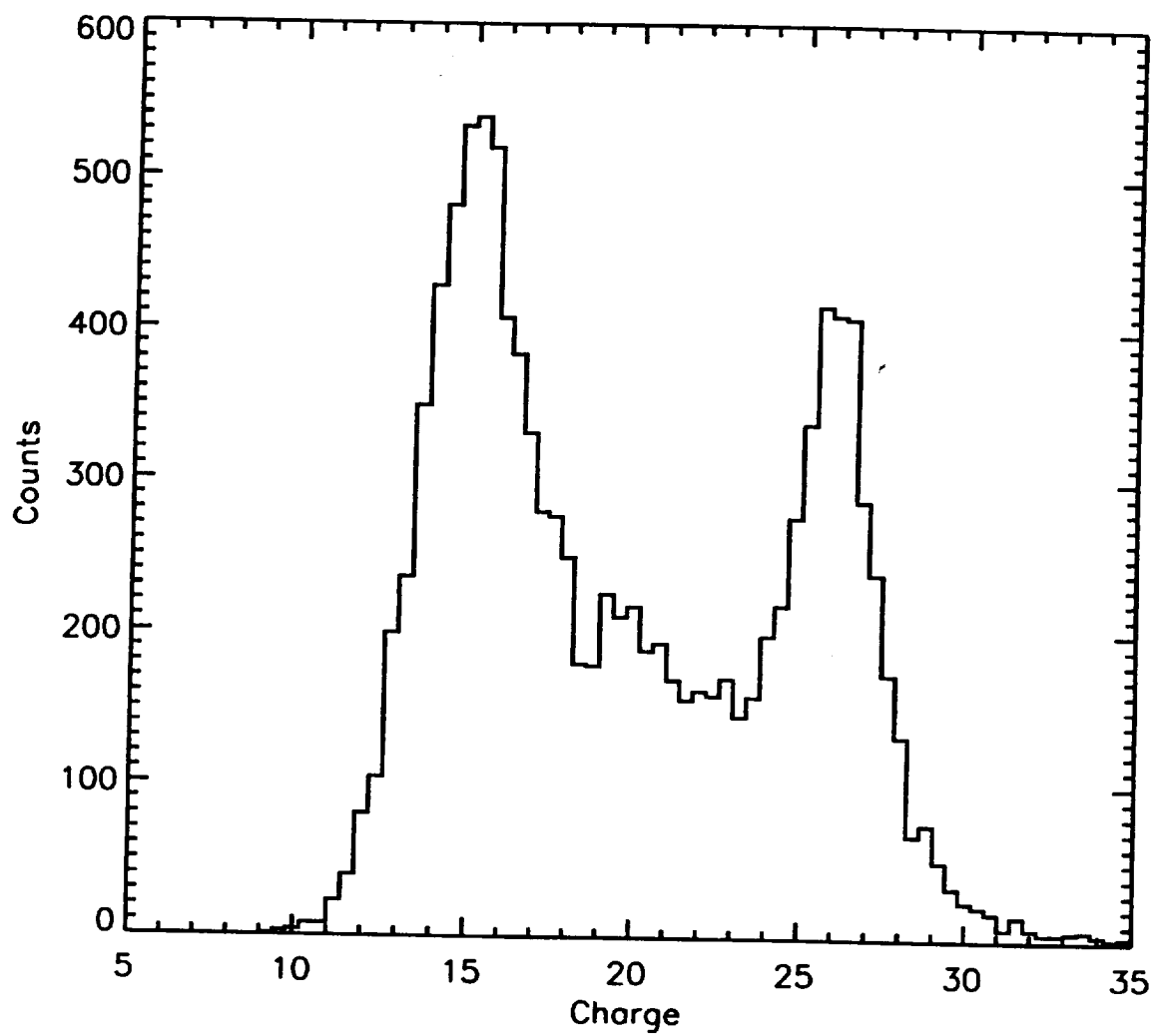viewing region A
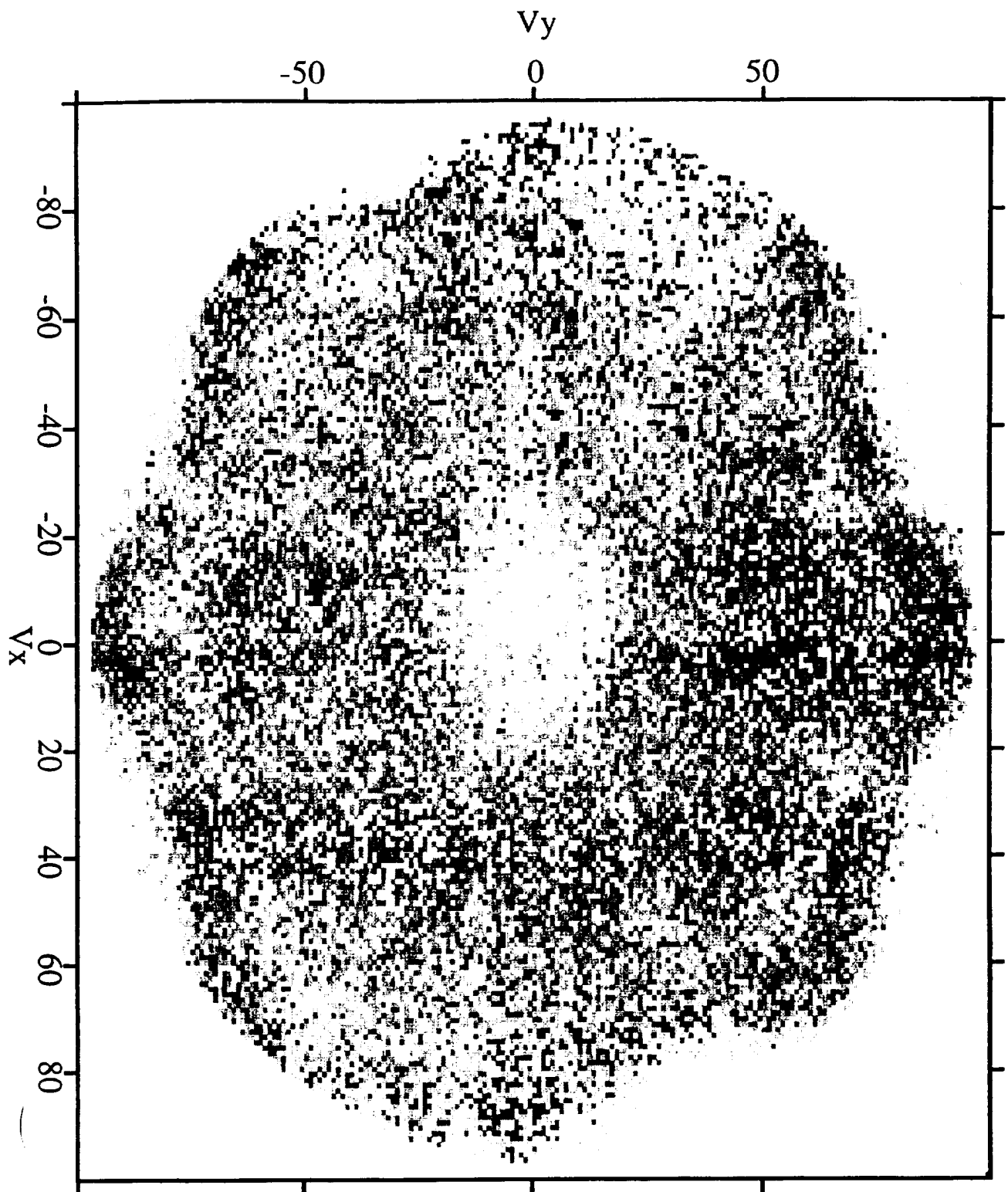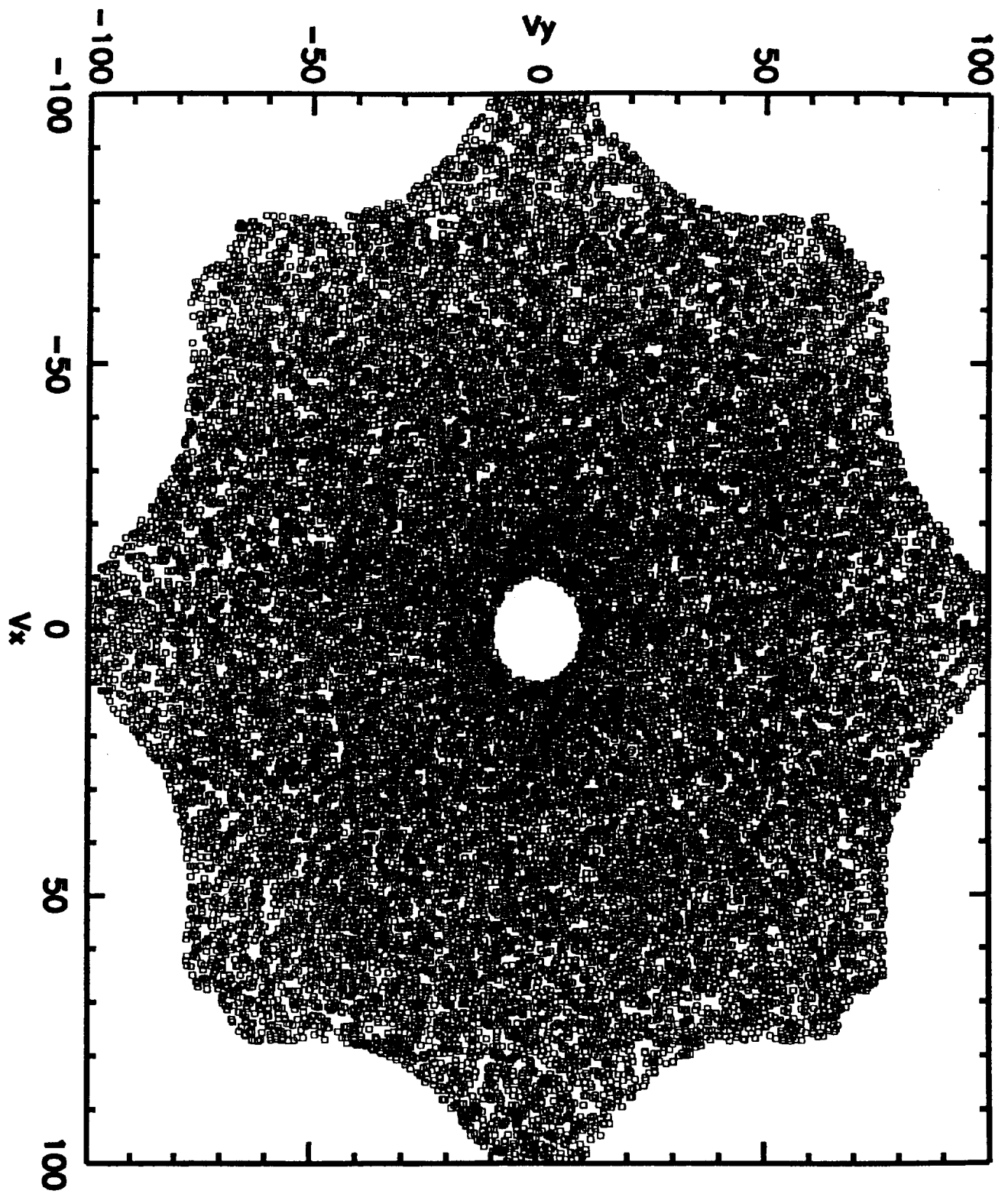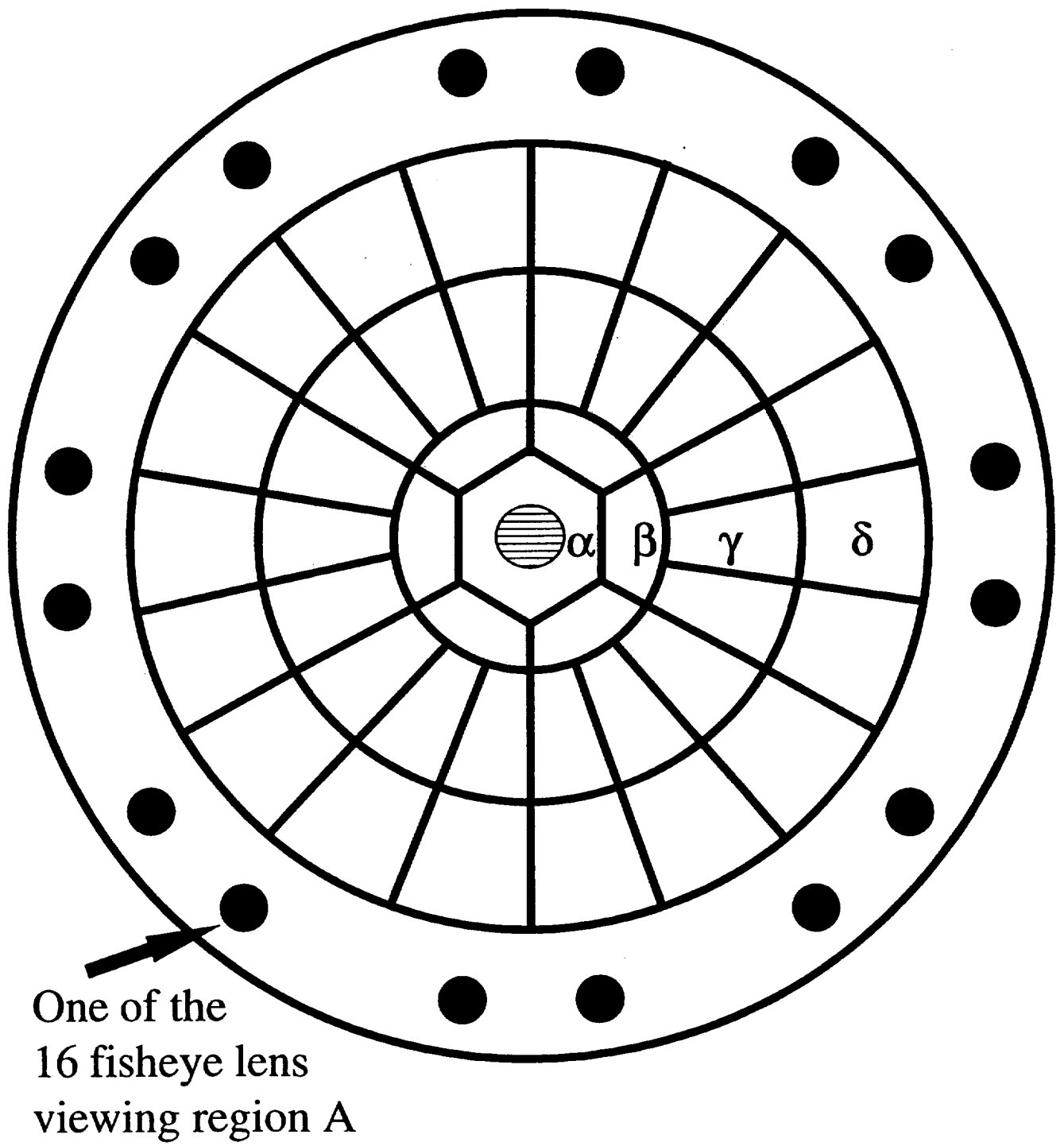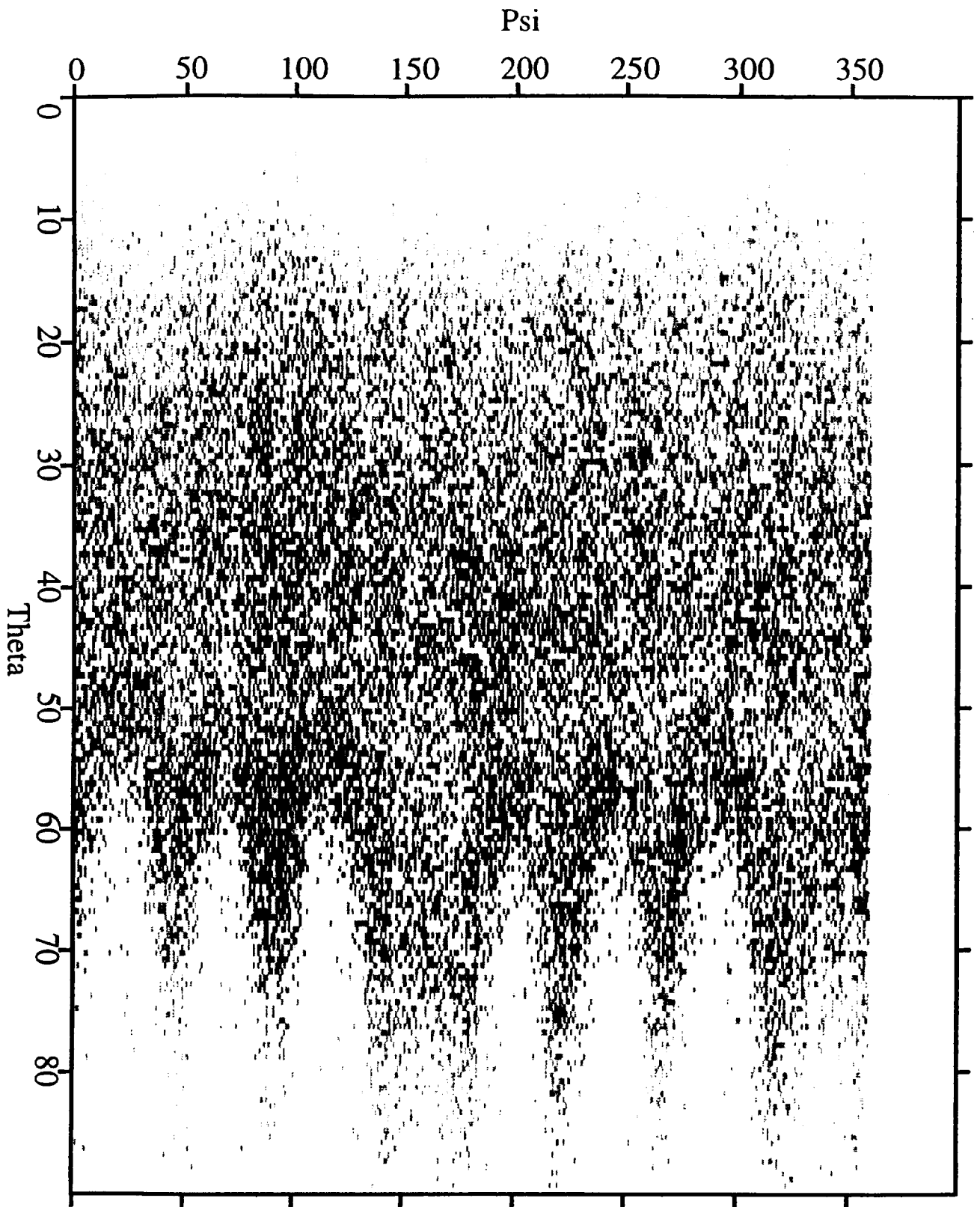
Figure 10
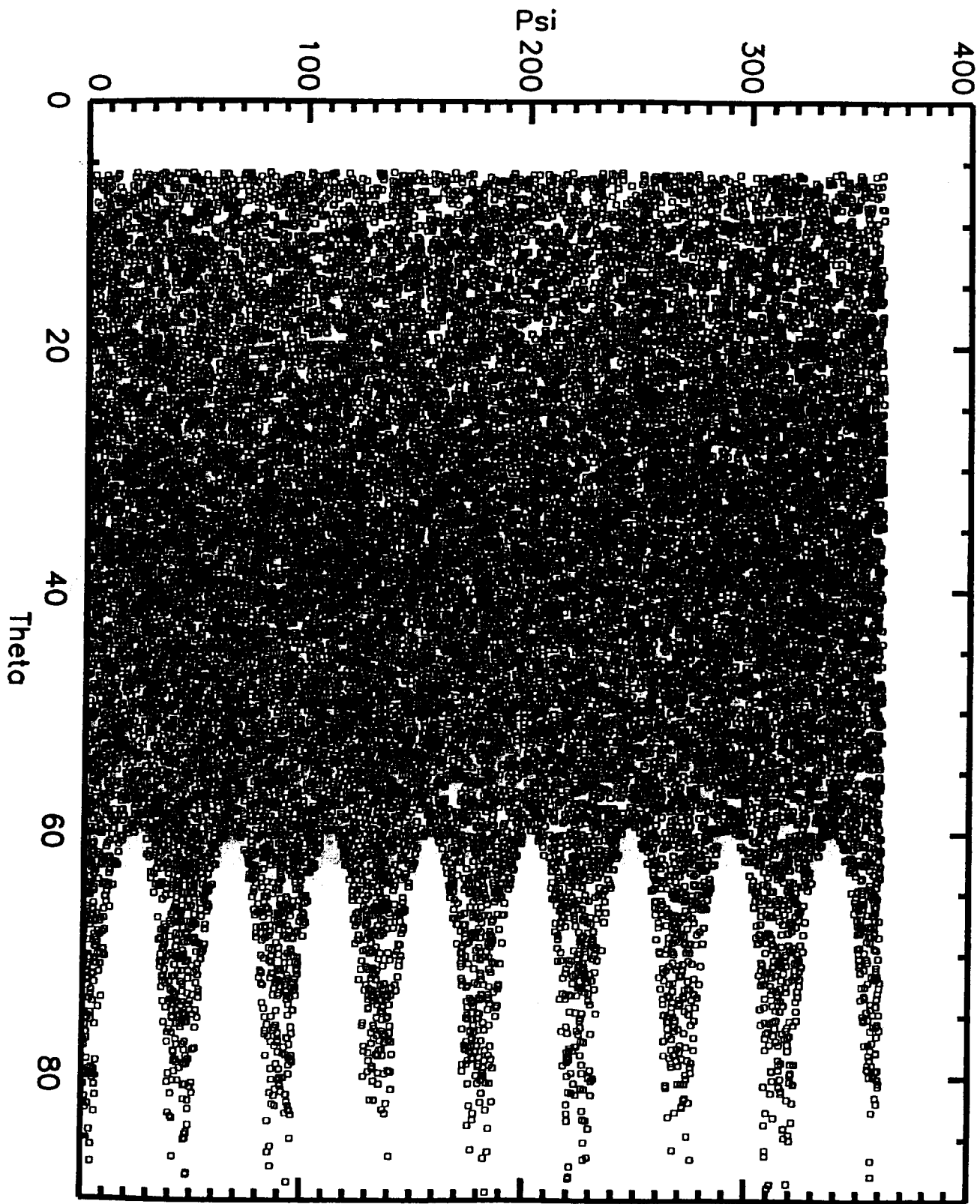
Figure 11a

Figure 11b
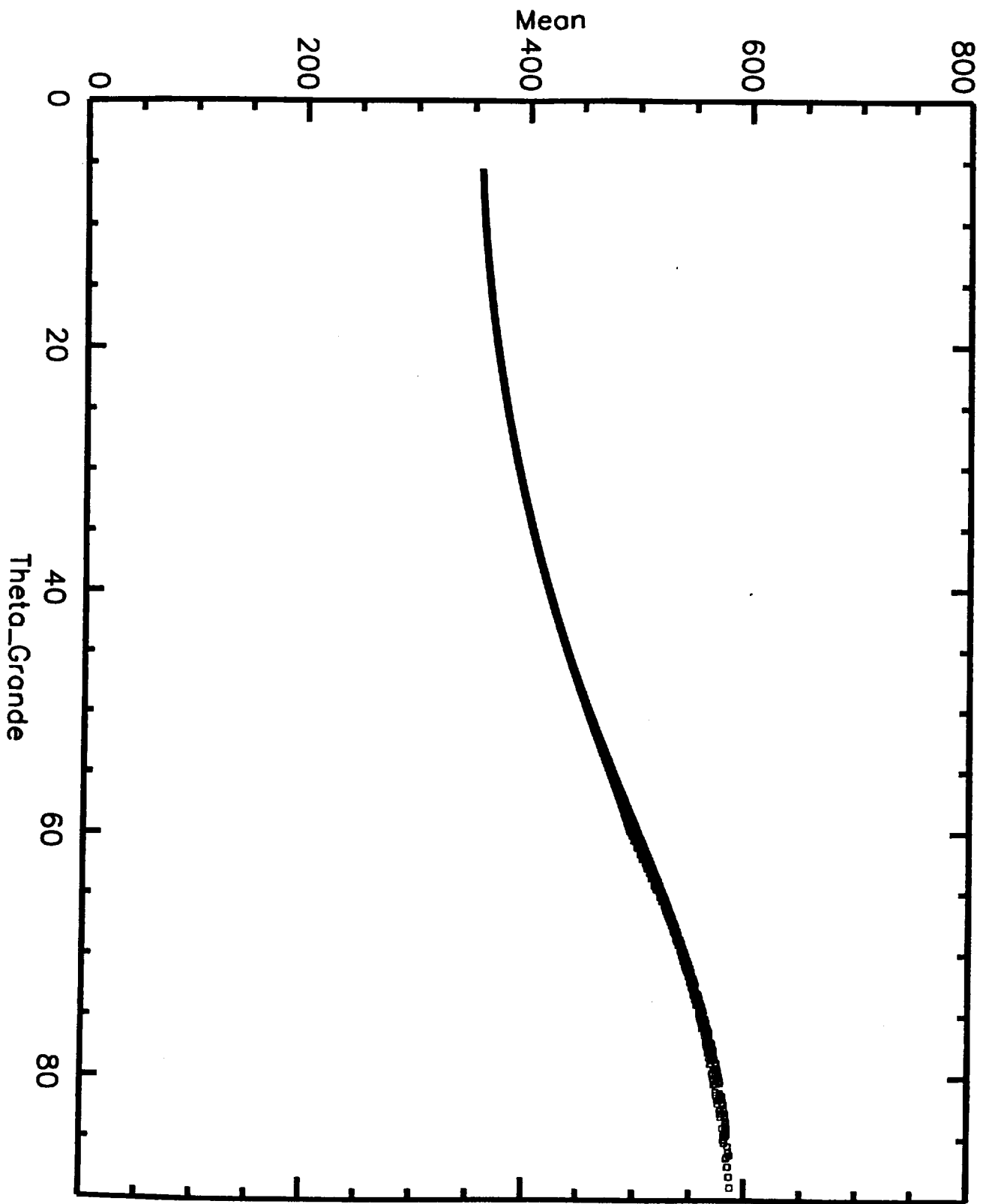
Figure 12
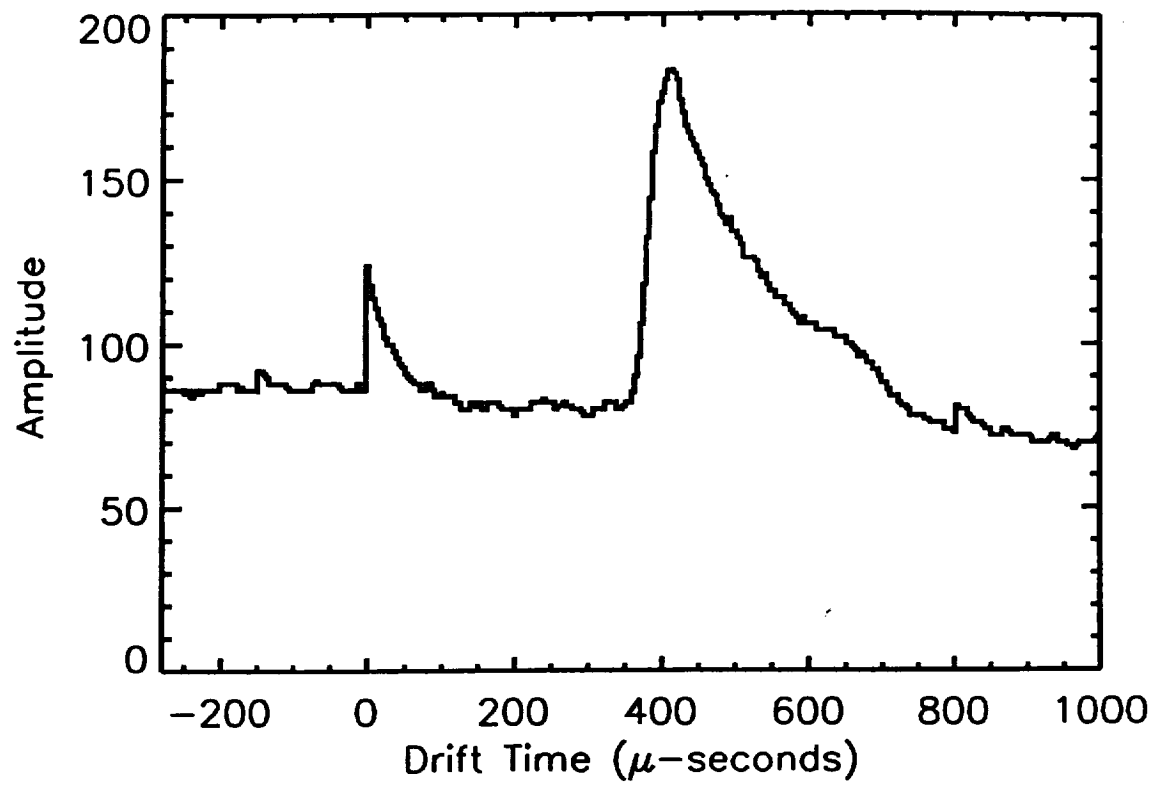
Figure 13a

Figure 13b

Figure 14

Counts

Impact Parameter

Figure 15a

Figure 15b

Access cover plate to top of the inner sphere

Flange

Top hat

Ceramic probe

Spacing and fixings (Only sample shown)

DETAIL A

3.0cm Gap

1.4 m

1 m

O ring seals

Flange

6mm of Pilot 425

Port holes for region B tube (8 in total)

Phototubes with fisheye lens (16 in total)

PM tube cans

Gas vent for C

Access plates (8 in total)

Outer belly band section

Closed spaced bolt pattern

Gas filling port for Region B

Welded flanges

Outer Sphere 3.5 mm thick (Grade N6) aluminum sections spun then welded

3.0cm Gap

1.5mm of Pilot 425

Inner belly band section

O ring seal

Spun from aluminum (Grade S1B) 0.47 cm thick at the pole and 0.31 cm at 75°

Gas filling port for Region C
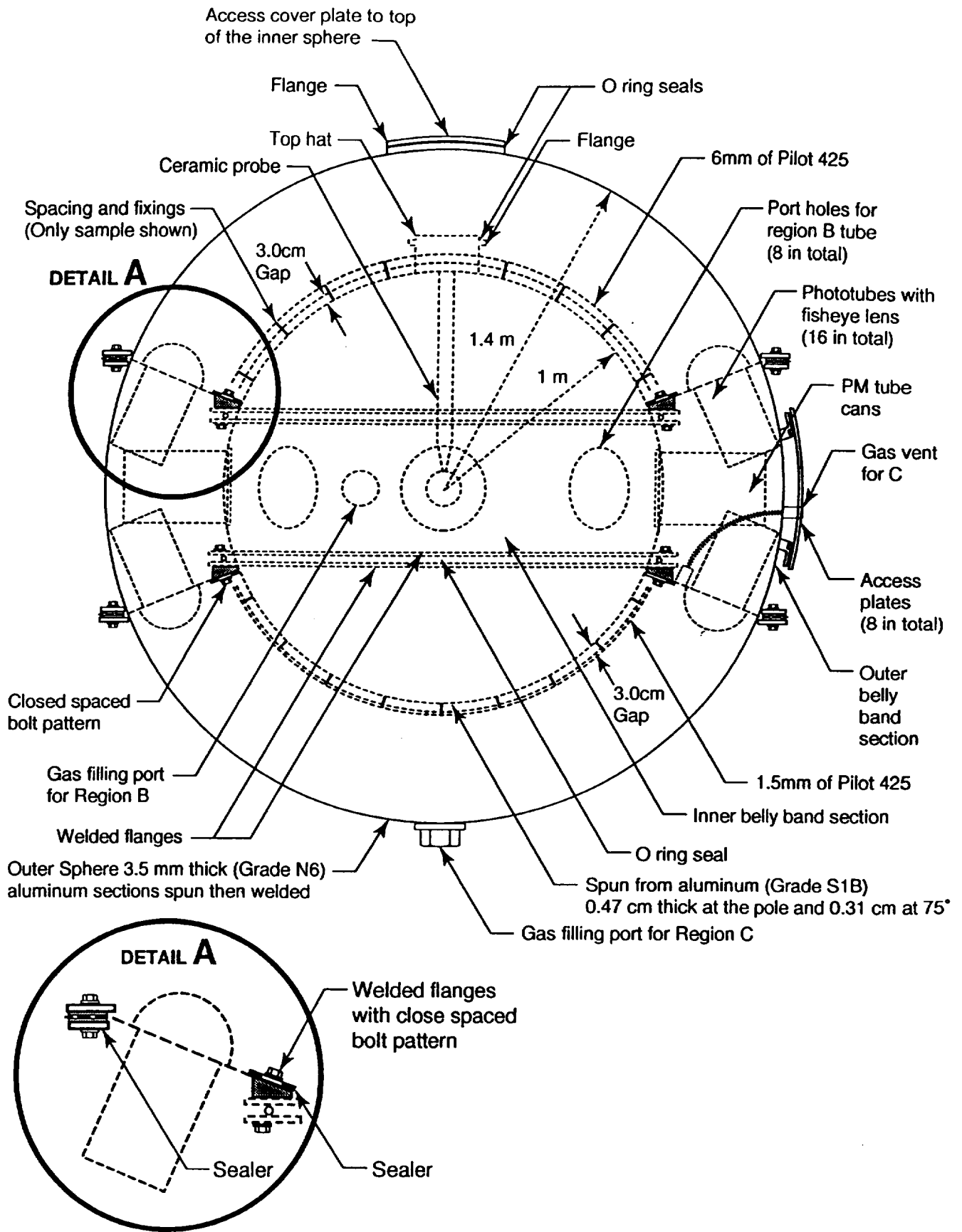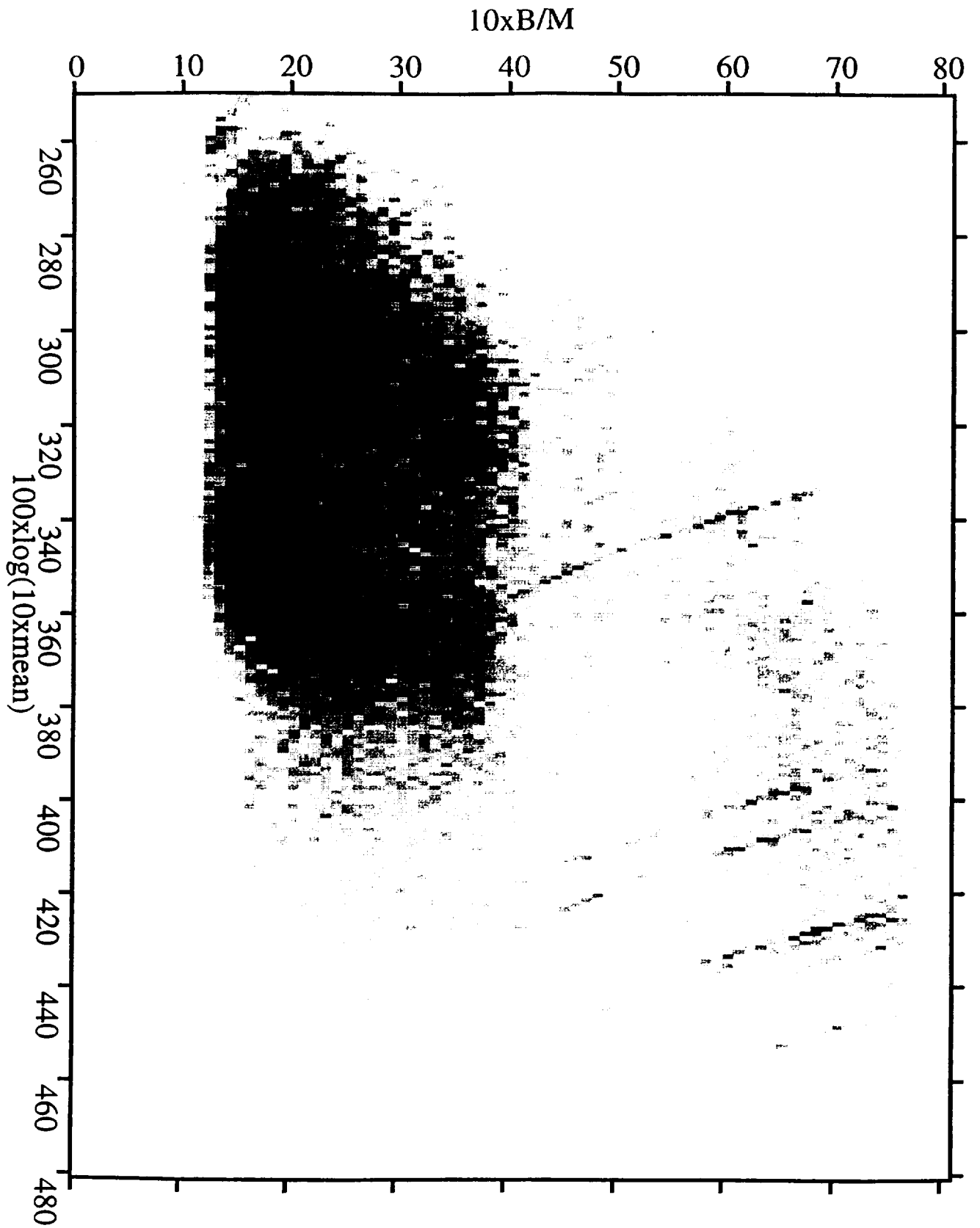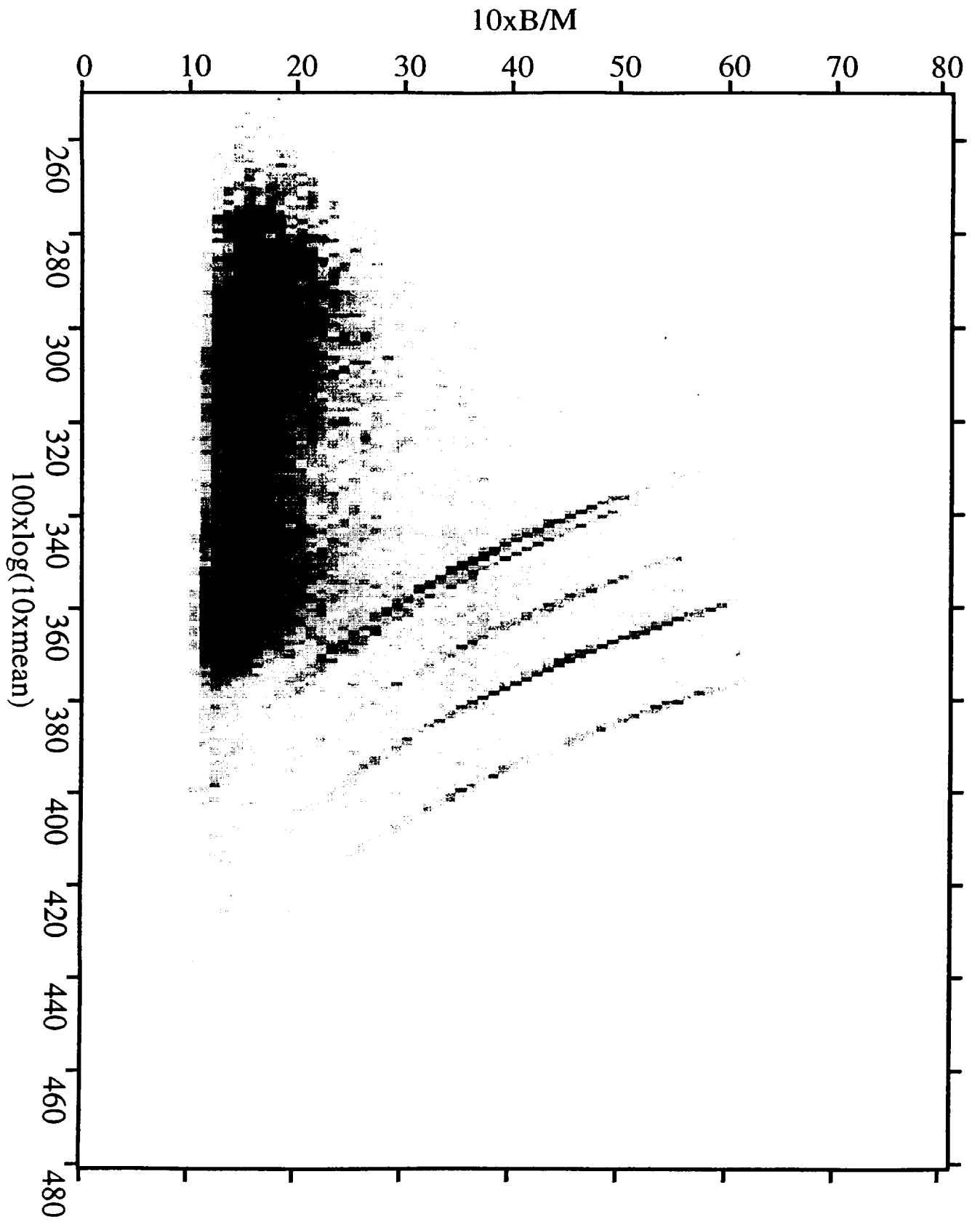
DETAIL A

Welded flanges with close spaced bolt pattern

Sealer   Sealer

5-23767

Figure 16

Figure 17

Figure 18